

AD-A127 845

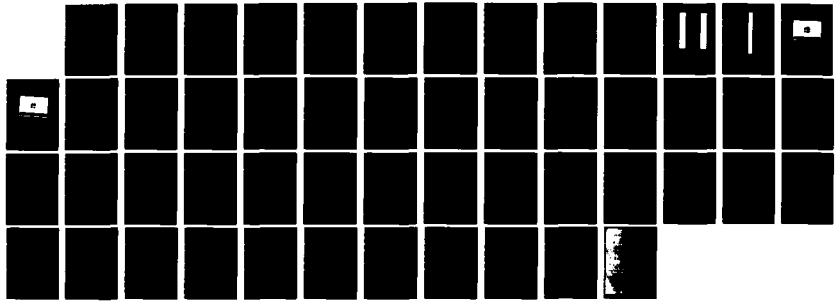
PULSED LASER DEVICE DEVELOPMENT DIAGNOSTIC TECHNIQUES
FOR PULSED LASER BEAM JITTER MEASUREMENT(U) AVCO
EVERETT RESEARCH LAB INC EVERETT MA T L CRONBURG
APR 82 DRAH01-80-C-0208

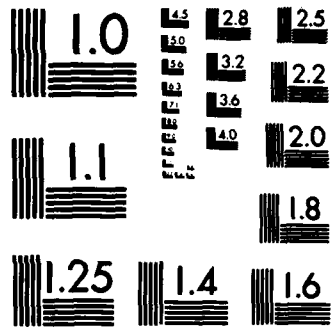
1/1

UNCLASSIFIED

F/G 20/5

NL





MICROCOPY RESOLUTION TEST CHART
NATIONAL BUREAU OF STANDARDS-1963-A

12

ADA 127845

PULSED LASER DEVICE DEVELOPMENT PROGRAM

**DIAGNOSTIC TECHNIQUES FOR PULSED LASER
BEAM JITTER MEASUREMENT**

T. L. Cronburg

AVCO EVERETT RESEARCH LABORATORY, INC.
a Subsidiary of the Avco Corporation
2385 Revere Beach Parkway
Everett, Massachusetts 02149

April 1982

Test Report
1 October 1981 - 30 January 1982

DTIC
SELECTED
MAY 10 1983
A

APPROVED FOR PUBLIC RELEASE; DISTRIBUTION UNLIMITED.

prepared for
HEADQUARTERS
U.S. ARMY MISSILE COMMAND
Redstone Arsenal, Alabama 35809

DTIC FILE COPY

88 05 09-135

UNCLASSIFIED

SECURITY CLASSIFICATION OF THIS PAGE (When Data Entered)

REPORT DOCUMENTATION PAGE		READ INSTRUCTIONS BEFORE COMPLETING FORM
1. REPORT NUMBER	2. GOVT ACCESSION NO. AD-A107945	3. RECIPIENT'S CATALOG NUMBER
4. TITLE (and Subtitle) PULSED LASER DEVICE DEVELOPMENT PROGRAM DIAGNOSTIC TECHNIQUES FOR PULSED LASER BEAM JITTER MEASUREMENT		5. TYPE OF REPORT & PERIOD COVERED TEST REPORT 10/1/81 - 1/30/82
7. AUTHOR(s) T. L. Cronburg		6. PERFORMING ORG. REPORT NUMBER
9. PERFORMING ORGANIZATION NAME AND ADDRESS Avco Everett Research Laboratory, Inc. 2385 Revere Beach Parkway Everett, MA 02149		8. CONTRACT OR GRANT NUMBER(s) DAAH01-80-C-0208
11. CONTROLLING OFFICE NAME AND ADDRESS Headquarters U.S. Army Missile Command Redstone Arsenal, AL 35809		10. PROGRAM ELEMENT, PROJECT, TASK AREA & WORK UNIT NUMBERS CDRL Item A008
14. MONITORING AGENCY NAME & ADDRESS (If different from Controlling Office)		12. REPORT DATE April 1982
		13. NUMBER OF PAGES
		15. SECURITY CLASS. (of this report) Unclassified
		15a. DECLASSIFICATION/DOWNGRADING SCHEDULE
16. DISTRIBUTION STATEMENT (of this Report) Approved for Public Release, Distribution Unlimited		
17. DISTRIBUTION STATEMENT (of the abstract entered in Block 20, if different from Report)		
18. SUPPLEMENTARY NOTES		
19. KEY WORDS (Continue on reverse side if necessary and identify by block number)		
Electric Discharge Laser		Visible Beam Characterization
Repetitively Pulsed		Infrared Beam Measurements
Beam Jitter Diagnostic		Gas Density Gradients
20. ABSTRACT (Continue on reverse side if necessary and identify by block number)		
<p>★ Beam jitter diagnostics were developed and tested on a repped-flowing CO₂ e-beam sustainer laser cavity. The limiting source of jitter was found to be due to gas density gradients in the cavity. Both flow-induced gradients and disturbances from the repped discharge contribute. Reduction of the jitter magnitude can be accomplished through temperature control of the gas flow and acoustic suppression. 7</p>		

DD FORM 1473 1 JAN 73 EDITION OF 1 NOV 68 IS OBSOLETE

UNCLASSIFIED

SECURITY CLASSIFICATION OF THIS PAGE (When Data Entered)

TABLE OF CONTENTS

<u>Section</u>		<u>Page</u>
1.0	INTRODUCTION	1
2.0	MEASUREMENT TECHNIQUES	3
	2.1 Infrared Measurement Technique	3
	2.2 Visible Characterization	9
3.0	PRELIMINARY TESTS	16
4.0	IR MEASUREMENTS	17
5.0	VISIBLE CHARACTERIZATION DATA	25
6.0	TEMPERATURE MEASUREMENTS	38
7.0	CONCLUSION	43



Accession For	
NTIS GRA&I	<input checked="" type="checkbox"/>
NTIS TAB	<input type="checkbox"/>
Unannounced	<input type="checkbox"/>
Justification	
Distribution/	
Availability Codes	
Avail and/or	
Special	

A

LIST OF ILLUSTRATIONS

<u>Figure</u>	<u>Page</u>
1. IR Jitter Measurement Configuration	4
2. Multiple IR Focal Images Recorded on Rotating Drum with Thermal Film	5
3. Multiple IR Focal Images at Reduced Beam Intensity	6
4. 10 x Enlargement of Pulse No. 15 of Figure 3	7
5. 10 x Enlargement of Pulse No. 16 of Figure 3	8
6. Visible Probe Beam Path	10
7. Reference Beam Path	12
8. Confocal Resonator Magnifies Jitter Angle by $R_1/(R_1 - R_2)$	14
9. IR Jitter Dependence on Cavity Flow Rate; Cavity Core Flow with Salt Windows	18
10. IR Jitter Dependence on Rep-Rate at Low Flow Rate; Cavity Core Flow with Salt Windows	19
11. IR Jitter Dependence on Rep-Rate at High Flow Rates (15-20 lbs/sec)	20
12. IR Jitter vs. Discharge Loading; Cavity Core Flow with Salt Windows	21
13. IR Jitter as Mufflers and Aerowindow are added to Coreflow	23
14. IR Jitter Dependence on Rep-Rate with Two Mufflers and Aerowindow	24
15. Cavity Beam During Flow Before First Pulse $\sigma_x = 3.09 \mu\text{rad}$, $\sigma_y = 7.13 \mu\text{rad}$, $\sigma_{\text{tot}} = 7.77 \mu\text{rad}$	26
16. Reference Beam Before First Pulse $\sigma_x = 2.30 \mu\text{rad}$, $\sigma_y = 2.15 \mu\text{rad}$, $\sigma_{\text{tot}} = 3.15 \mu\text{rad}$	27

<u>Figure</u>	<u>Page</u>
17. Pulse-to-Pulse Cavity Beam Jitter	29
18. Recovery of Cavity Beam After First Pulse	30
19. Pulse-to-Pulse rms Jitter of Visible Probe Beam vs. Flow Rate	32
20. Visible Probe Beam Jitter Corrected by Confocal Resonator Factor of 1.75	33
21. Comparison of IR Jitter With Visible Jitter	34
22. Effect of Repped Discharge on Visible Beam Jitter	35
23. Visible Probe Beam Jitter as Mufflers and Aerowindow are Added	36
24. Humdinger Gas System	39
25. Differential Thermocouple Recording, Horizontal Displacement	40
26. Differential Thermocouple Recording, Vertical Displacement	41

1.0 INTRODUCTION

The term beam jitter refers to pulse-to-pulse directional variation of the repetitively-pulsed laser beam. The mechanisms causing angular deflection of one pulse relative to another may be random or ordered. The importance of the angular jitter is that the central peak of the focused beam will not be stationary in the focal plane but move from pulse-to-pulse distributing the repped laser flux over an enlarged area. When the jitter is a significant fraction of the peak width the effectiveness of the flux is reduced.

The purpose of this test program was to develop and test techniques for measuring pulse-to-pulse beam jitter for ABEL-type CO₂ lasers. The jitter magnitude for various conditions in a repped flowing cavity was to be measured to determine the sensitivity to various laser parameters and design variables. The data was to be used to identify and discriminate between the possible sources of beam jitter.

Tests were performed using the Humdinger laser which has the same basic flow geometry as ABEL.

The tests consisted primarily of two types: IR jitter measurements and visible beam characterization. The IR measurements were direct measurements of the pulsed 10.6 μm beam extracted from the laser cavity with an unstable resonator. The visible characterization tests used a visible wavelength cw laser beam to probe the laser cavity and beam path for simulation of the IR beam steering effects. An external reference beam was also used to monitor mirror stability and potential beam deflections in the external beam path in the room air.

Using the measurement techniques described here, displacement of the focal spot, a small fraction of a peak width, were measured. Approximately $\pm 5 \mu\text{rad}$ was resolved for peaks having a (half-power) radius of 120 μrad .

The tests reported here looked at an apertured portion of the Humdinger output beam. The IR data were taken mostly with a 4.5 cm round aperture and a few runs with a 9.0 cm aperture. The difference between the 4.5 cm and 9.0 cm data was less than the shot-to-shot variation or scatter in the data. The 4.5 cm aperture data were slightly more symmetric and thus easier to measure. It was therefore used to survey the beam motion under the various conditions.

The visible beam measurements were taken with a small (1.2 cm diameter) aperture and yet the magnitudes of the jitter measured this way were very similar to the IR data with large apertures (4.5-9 cm). Our experience on this device indicates that the jitter is a very weak function of aperture size.

The laser components consisting of core cavity, mufflers and aerowindow were tested at various flow rates, rep-rates and power levels. The results were that except for an anomalous problem (presumably easily correctable) with one of the mufflers, the beam jitter was dominated by refractive effects in the core laser cavity. A baseline jitter of about 20 μ rad was observed, which increased for high flow rates and high rep rates (30-50 pps).

The visible probe beam tests demonstrated that the beam jitter is not caused by air breakdown or thermal blooming effects of the high-power IR beam. The probe beam also made it possible to sample times between the laser discharge pulses and during the flow before pulsing starts.

The tests indicate that both gas flow and disturbances from the previous discharge pulses are contributors to jitter. The flow-only component limits the single pulse beam pointing precision. The flow only refractive variations are presumably thermal, so some temperature measurements of the gas at different points in the flow system were made. These are discussed in Section 6.0.

2.0 MEASUREMENT TECHNIQUES

Two types of jitter diagnostic techniques were developed and tested. One measures the infrared (10.6 μm) beam jitter directly and the other involves a visible beam characterization of the laser cavity using a probe beam (at 0.633 μm). A second probe beam was also used as a reference monitor for mirror vibration and beam steering due to density gradients in the room air.

2.1 INFRARED MEASUREMENT TECHNIQUE

The beam path for the infrared (IR) beam jitter measurements is shown in Figure 1. A circular aperture (between 4.5 and 9 cm diameter) was used to define the beam cross section. A 16-m focal length mirror was used to focus the beam. The beam was recorded at the focal plane with thermal sensitive film on a rotating drum. The angular velocity of the rotating drum was adjusted to record up to 20 pulses on the circumference of the drum during one revolution. Stationary crosshairs were positioned 1-2 mm in front of the rotating drum surface. The 0.001 in. crosshairs left a shadow in the recorded images which was used as a coordinate system for measuring the position of the center of each focal image.

A recorded IR pulse train is reproduced in Figure 2. The coordinates of the spots were measured using a strip projector to magnify the images 20 times. The center of the image on the screen was determined manually by fitting a circle to the inner ring in the pattern with a compass. The X and Y coordinates of this center were then measured in mm relative to the crosshair. The best measurement precision was obtained by reducing the exposure intensity on the film as in Figure 3. The beam intensity was varied using attenuators inserted in the beam in front of the aperture. Two types of attenuators were used. One is a transmission grating consisting of a linear array of copper wires. The transmission can be varied by adjusting the effective number of wires/in. from 20 to 60. Two orthogonal arrays of this type were used. The second type of attenuator is a transmission grating consisting of a two-dimensional array of circular holes in a copper sheet. Fixed near-field transmissions of 8, 14, 33 and 50 percent were available. The far-field transmission is equal to the square of the near-field transmission.

At reduced exposure the precision of the measurements of the magnified (20 X) images was $\pm 1/20$ mm which corresponds to ± 3.4 μrad . Figures 4 and 5 show two of the pulses from Figure 3 magnified. It is apparent from the position of the spots relative to the crosshair shadow that the beam axis has shifted from one pulse to the next.

For each series of pulses the X and Y measurement were averaged to find the mean coordinates. Then the standard deviation σ_x and σ_y were calculated for the run. The rms angular deviation θ_x , θ_y were then given by

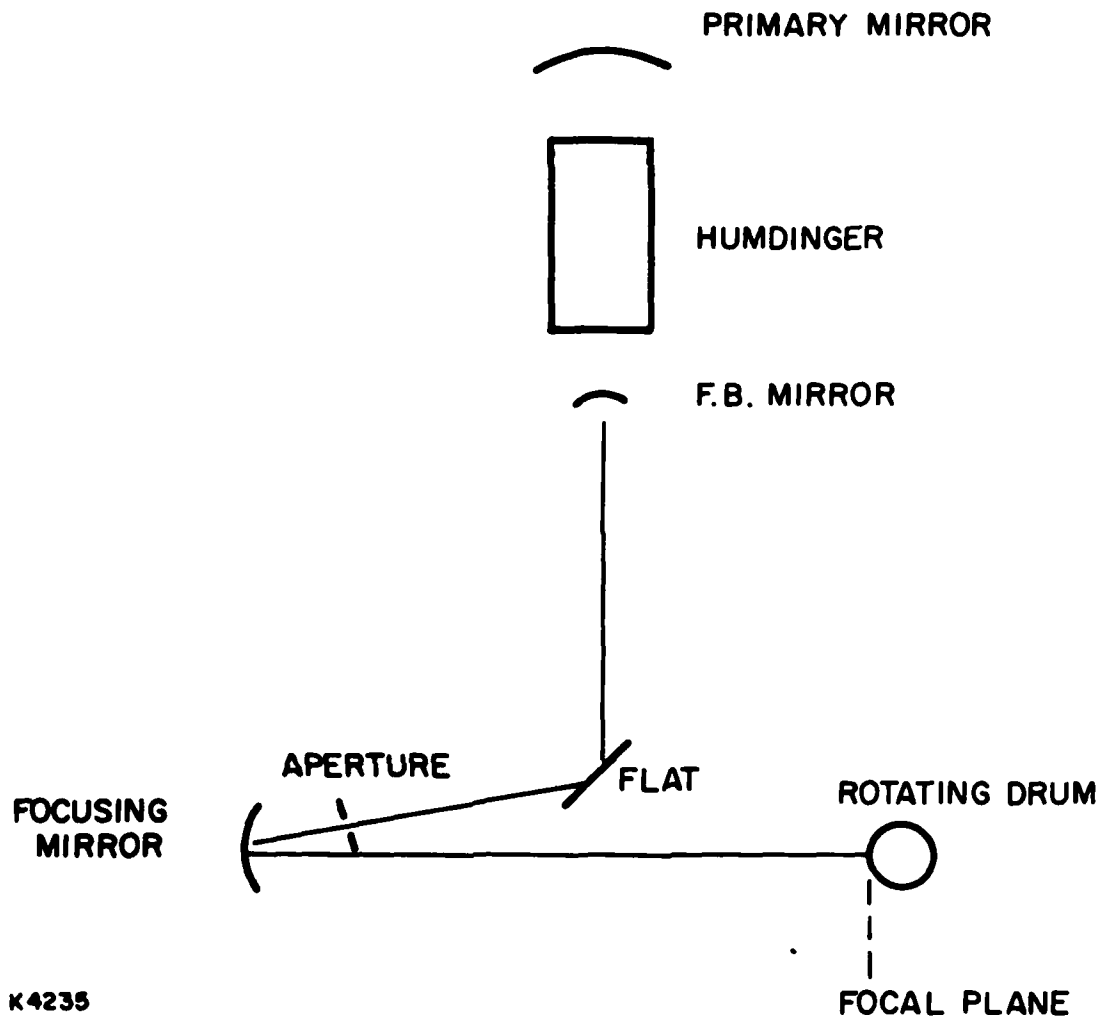
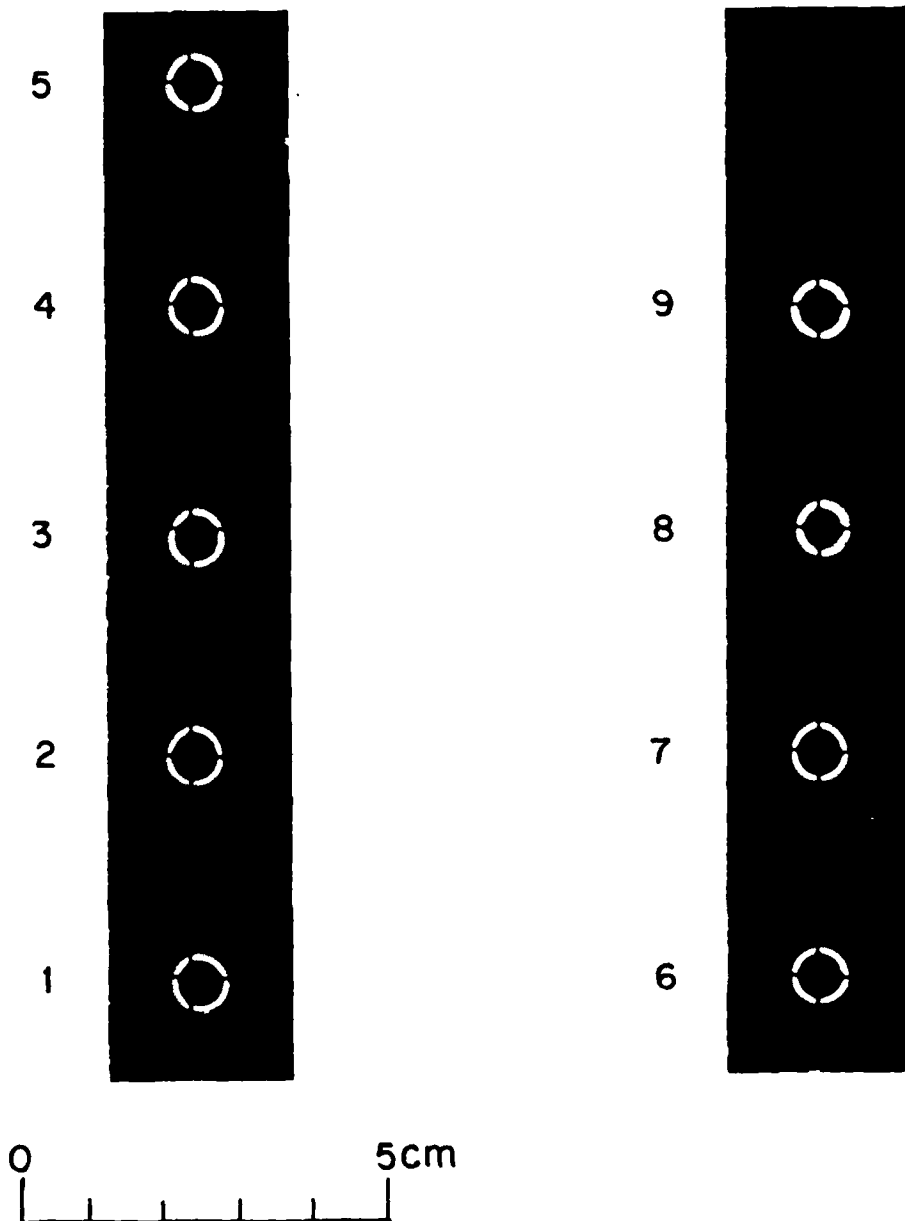


Figure 1. IR Jitter Measurement Configuration. Focal Length is 16 m.

PULSE #



K4241

Figure 2. Multiple IR Focal Images Recorded on Rotating Drum with Thermal Film. Figure is a contact print of the film. The bright ring in the images results from the characteristics of the film. The outer diameter corresponds to the film threshold of 0.90 J/cm^2 . Above 5 J/cm^2 the image is bleached resulting in the dark center.

PULSE #

18

17

16

15

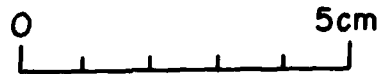
14

13

12

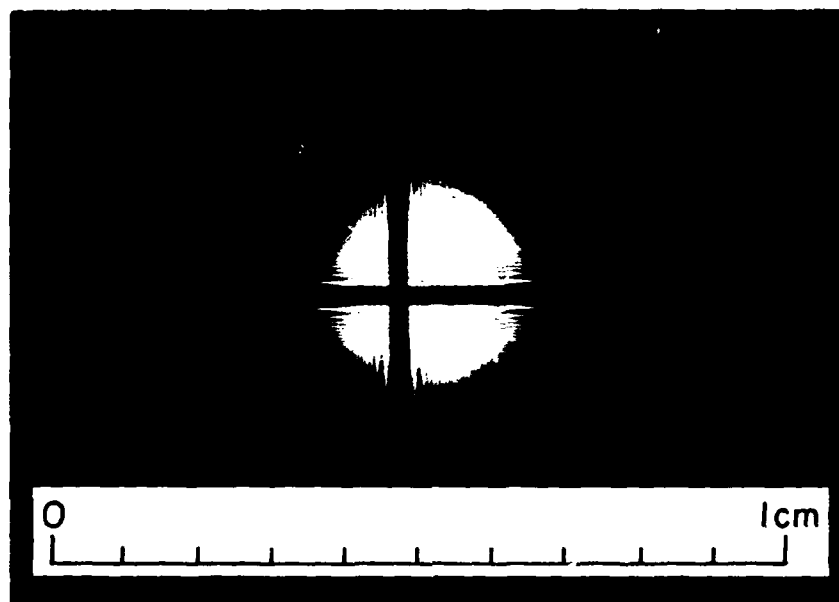
11

10



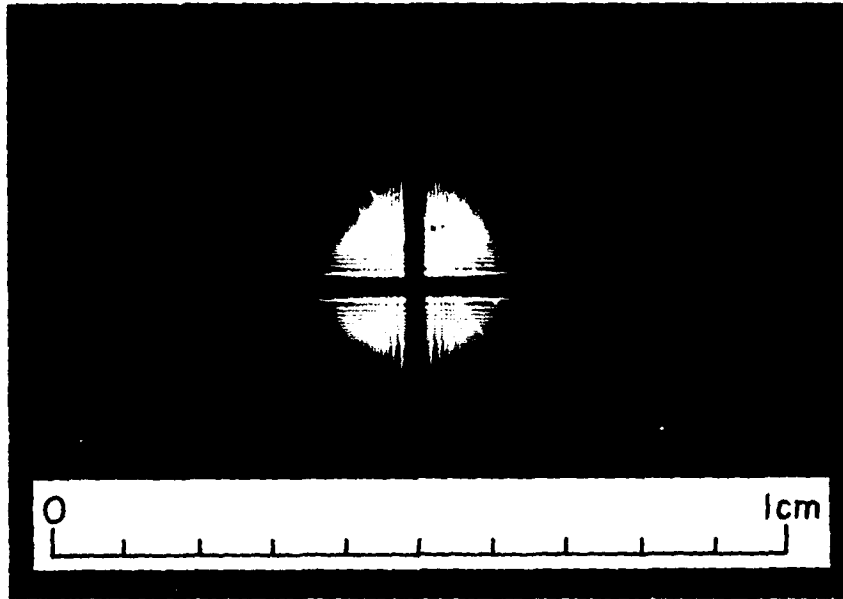
K4218

Figure 3. Multiple IR Focal Images at Reduced Beam Intensity. 4.5 cm aperture results in a airy spot diameter of 0.93 cm (at dark rings). Only peak intensity is recorded on film.



K4219

Figure 4. 10 x Enlargement of Pulse No. 15 of Figure 3. Each division on scale corresponds to $67.5 \mu\text{rad}$.



K4220

Figure 5. 10 x Enlargement of Pulse No. 16 of Figure 3. Beam has moved $25 \pm 3 \mu\text{rad}$ to left compared to Pulse No. 15.

$$\theta_x = \frac{\sigma_x}{f}$$

$$\theta_y = \frac{\sigma_y}{f}$$

where the focal length f is 16 m. The total rms jitter of the beam is then given by

$$\theta = \sqrt{\theta_x^2 + \theta_y^2}$$

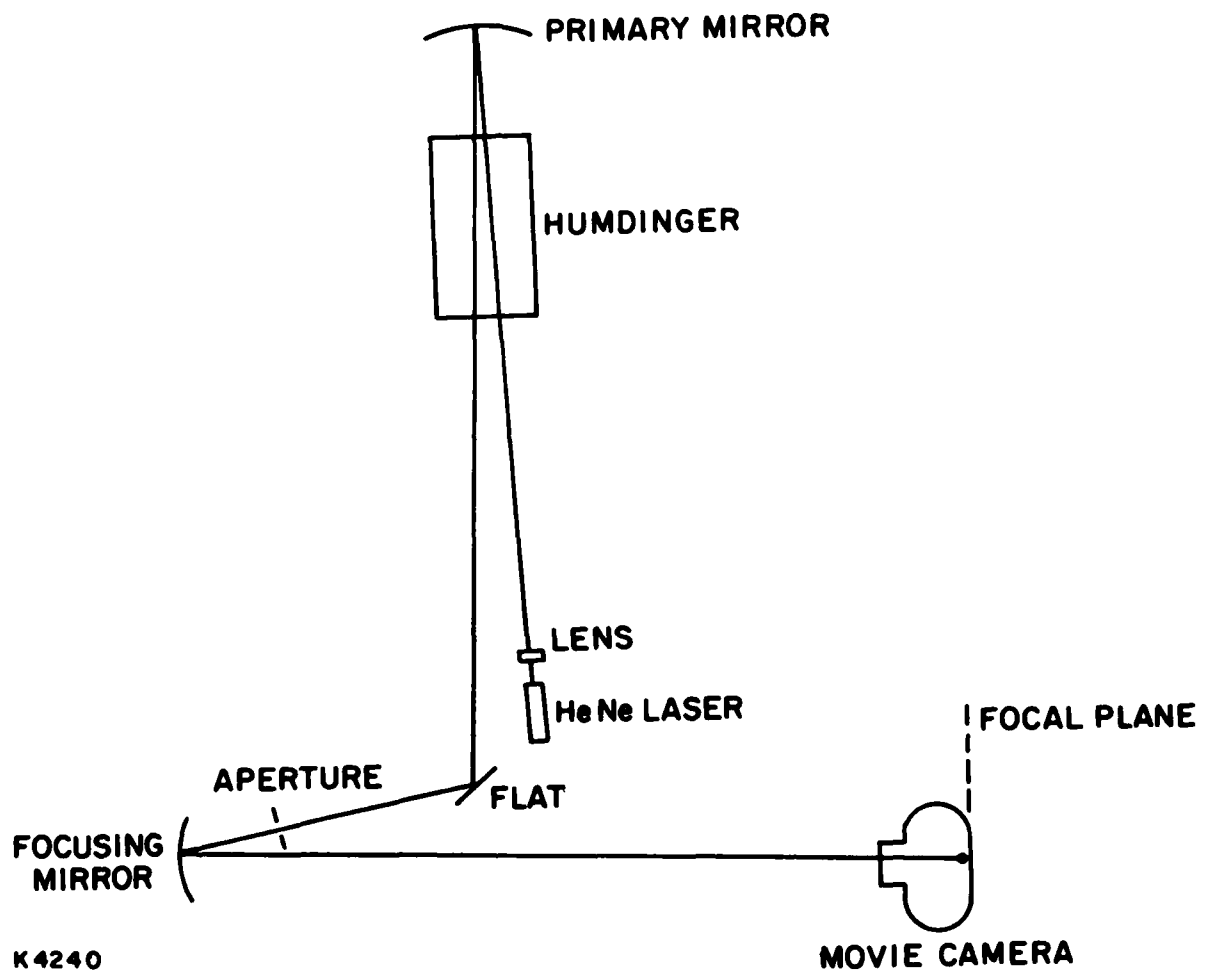
The IR jitter data measured under a number of different conditions is discussed in Section 4.0.

2.2 VISIBLE CHARACTERIZATION

A visible wavelength ($0.633 \mu\text{m}$) beam of light was used to characterize the laser cavity under flowing and discharge conditions. The refractive beam deflection effects do not scale with wavelength, but with the index of refraction of the gas. Since the index at $10.6 \mu\text{m}$ is virtually the same as at $0.633 \mu\text{m}$ the magnitude of the visible beam jitter is the same as the IR jitter. This technique is useful for investigating flow contributions to jitter, beam motion between pulses, and the frequency spectrum of induced beam motion. It can be used to differentiate high-power air breakdown heating effects, and thermal blooming or nonlinear absorption in the beam path because these effects would be eliminated with the low power visible beam.

The configuration used for the visible beam measurements is diagrammed in Figure 6. The beam makes a double pass through the laser cavity. The same flat and focusing mirror used for the IR measurements were used. The focal images were recorded with a Hy-Cam movie camera with an adjustable framing rate up to 10,000 fps. For these tests framing rates of 1000-4000 fps were used. In addition a TV camera and video recorder were used to record some of the data. The TV was useful in setting up the experiment, eliminating vibrations in the optics and tracking down thermal gradients in the room. However, the higher framing rates of the Hy-Cam made it more suitable for recording the laser cavity jitter data (the TV camera framing rate is only 60 Hz).

The movie camera was used without a lens so as to record the focal spots directly on the film. Crosshairs were mounted on the camera aperture. The shadow of the crosshairs in the focal image was used as a coordinate system for measuring the position of the center of each image on the film. The images were projected on a screen at 50 X and the coordinates of each spot measured as for the IR images discussed earlier.



K4240

MOVIE CAMERA

Figure 6. Visible Probe Beam Path. Probe beam has virtual focus at focal plane of primary mirror. Collimated beam is apertured to 1.3 cm diameter.

A second visible light beam was used as a reference beam for monitoring mirror stability and disturbances from thermal gradients in the room air along the beam path. The beam path for the reference beam is illustrated in Figure 7. The reference beam senses all the mirrors in the optical system without going through the laser cavity. The reference beam passed through the same aperture used for the cavity beam. A prism was used to deflect the reference beam into the movie camera so that both beams could be recorded simultaneously.

For a circular aperture the dark ring in the Fraunhofer diffraction pattern subtends an angle θ , given by

$$\theta = 2.44 \frac{\lambda}{d}$$

where λ is the wavelength of the light and d is the diameter of the aperture. A 1.3 cm aperture was used with the visible beam and a 4.5 cm aperture with the IR. The size of the airy pattern is summarized in Table 1 and compared with the IR airy pattern.

The visible probe beam jitter measurements must be adjusted before comparing them with the IR jitter data. The deflection angles introduced by the laser cavity are magnified by the confocal resonator. The schematic diagram in Figure 8 compares the deflection of the probe beam with that of the oscillator (IR beam). Any beam steering in the laser can be treated as tilt in the primary mirror M_1 . Assume M_1 is tilted through an angle θ . Then the probe beam is deflected through an angle 2θ .

$$\alpha_s = 2\theta$$

The resonator axis on the other hand is determined by a line connecting the centers of curvature of the two mirrors. When the primary mirror M_1 is tilted through an angle θ its center shifts from C_1 to C_1' a distance $R_1\theta$. The oscillator axis is thus shifted through an angle α_{osc} where

$$\alpha_{osc} = \frac{R_1\theta}{D}$$

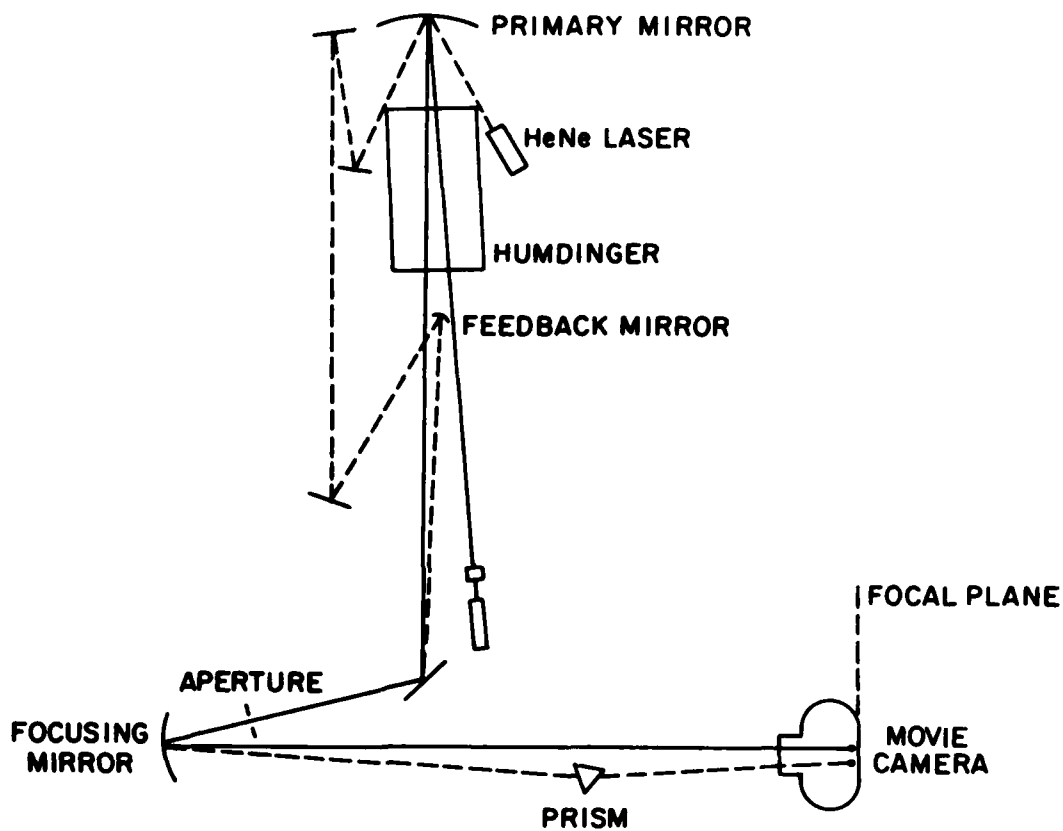
For a confocal resonator both mirrors have a common focus at f halfway between each mirror and its center of curvature hence,

$$D = \frac{R_1}{2} - \frac{R_2}{2}$$

Thus

$$\alpha_{osc} = \frac{2 R_1 \theta}{R_1 - R_2}$$

REFERENCE BEAM - - - - -
CAVITY BEAM - - - - -



K4237

Figure 7. Reference Beam Path. Beam senses all mirrors in the system without going through laser cavity. Thermal gradients in room air are also detected.

TABLE 1. FOCAL SPOT CHARACTERISTICS

λ	APERTURE DIA	DARK RING		HALF-POWER POINT "RADIUS"	90 PERCENT POWER POINT "RADIUS"
		"DIA"	"RADIUS"		
10.6 μm	9 cm	290 μrad	145 μrad	60 μrad	24 μrad
	4.5	580	290	120	49
0.633 μm	1.3	118	59	24	20

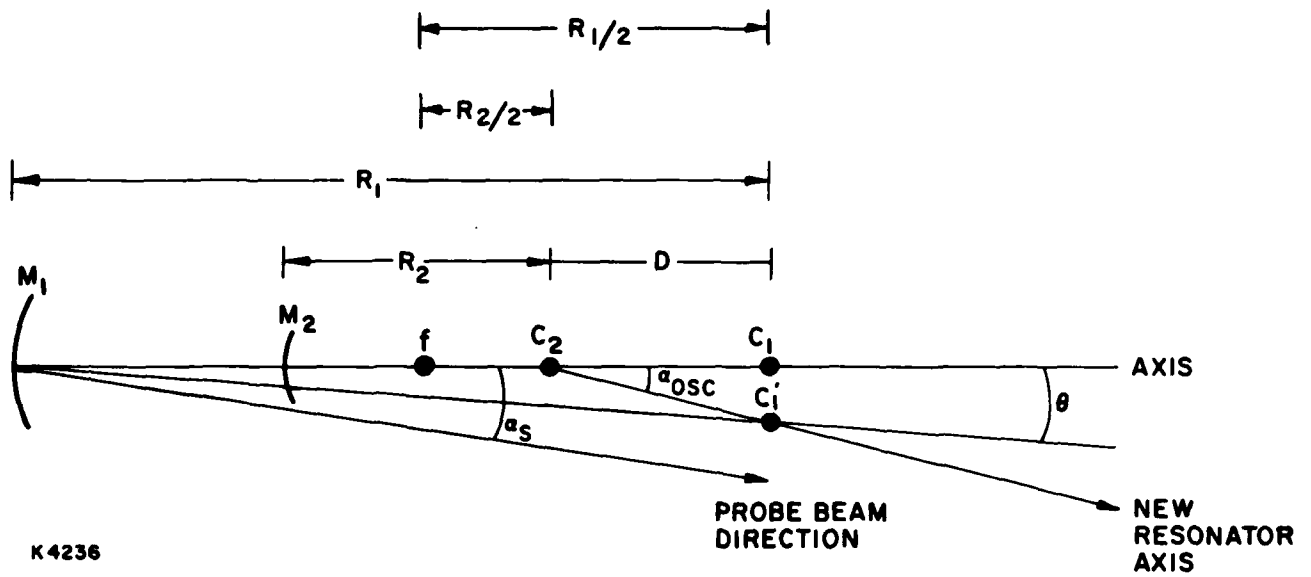


Figure 8. Confocal Resonator Magnifies Jitter Angle by $R_1/(R_1 - R_2)$

Replacing θ with $\alpha_s/2$ we obtain the relationship between the probe beam deflection and the oscillator deflection,

$$\alpha_{osc} = \frac{R_1}{R_1 - R_2}$$

For Humdinger

$$R_1 = 28 \text{ m}$$

$$R_2 = 12 \text{ m}$$

$$\alpha_{osc} = 1.75 \alpha_s$$

The probe beam jitter measurements must therefore be multiplied by 1.75 to project the magnitude of jitter which would result when the oscillator is used.

3.0 PRELIMINARY TESTS

A number of preliminary tests were performed prior to detailed IR and visible jitter measurements of the laser cavity in the various configurations. These tests involved visible cavity beam and reference beam tare measurements without flow or discharge to check out the stability of the system. These were followed by reference beam tests with flow and then with discharge. During these tests one of the mirrors in the reference leg was found to vibrate ($\sim 10 \mu\text{rad}$) during gas flow. This was eliminated by mounting on rubber. No vibration of the mirrors for the cavity beam was detected.

The limitation on the stability of the system was found to be deflection from thermal gradients in the room air. By turning off the building heating system the baseline jitter (for both the probe beam and the reference beam) was reduced from 10-15 μrad to 3-5 μrad . Therefore, all the subsequent tests were performed with the heating system blowers turned off.

The stability of the tare cavity beam and the reference beam during flow and discharges established that the beam jitter observations in Sections 4.0 and 5.0 are dominated by the laser itself. The reference beam was monitored during the visible characterization studies in Section 5.0 but not during the IR studies in Section 4.0. Some detailed measurements and analysis of the reference beam are presented in Sections 5.0 and 6.0. The tests with the reference beam demonstrated that vibrations from laser pulsing and flow did not move the mirrors in the system and that the effects measured are predominantly the effects of the gas medium on the laser beam.

4.0 IR MEASUREMENTS

Using the measurement techniques presented in Section 2.1, the contributions to the IR jitter of each laser component was tested. First, the core cavity with two salt windows was tested. Then one muffler (at the aerowindow end) was added. The aerowindow was then added. Next the second muffler was added. When the first muffler was added the salt window was moved from the core cavity to the outside of the muffler. When the aerowindow was added the salt window was removed. The second salt window was removed when the second muffler was added.

The IR tests were performed primarily with the gas mixture:

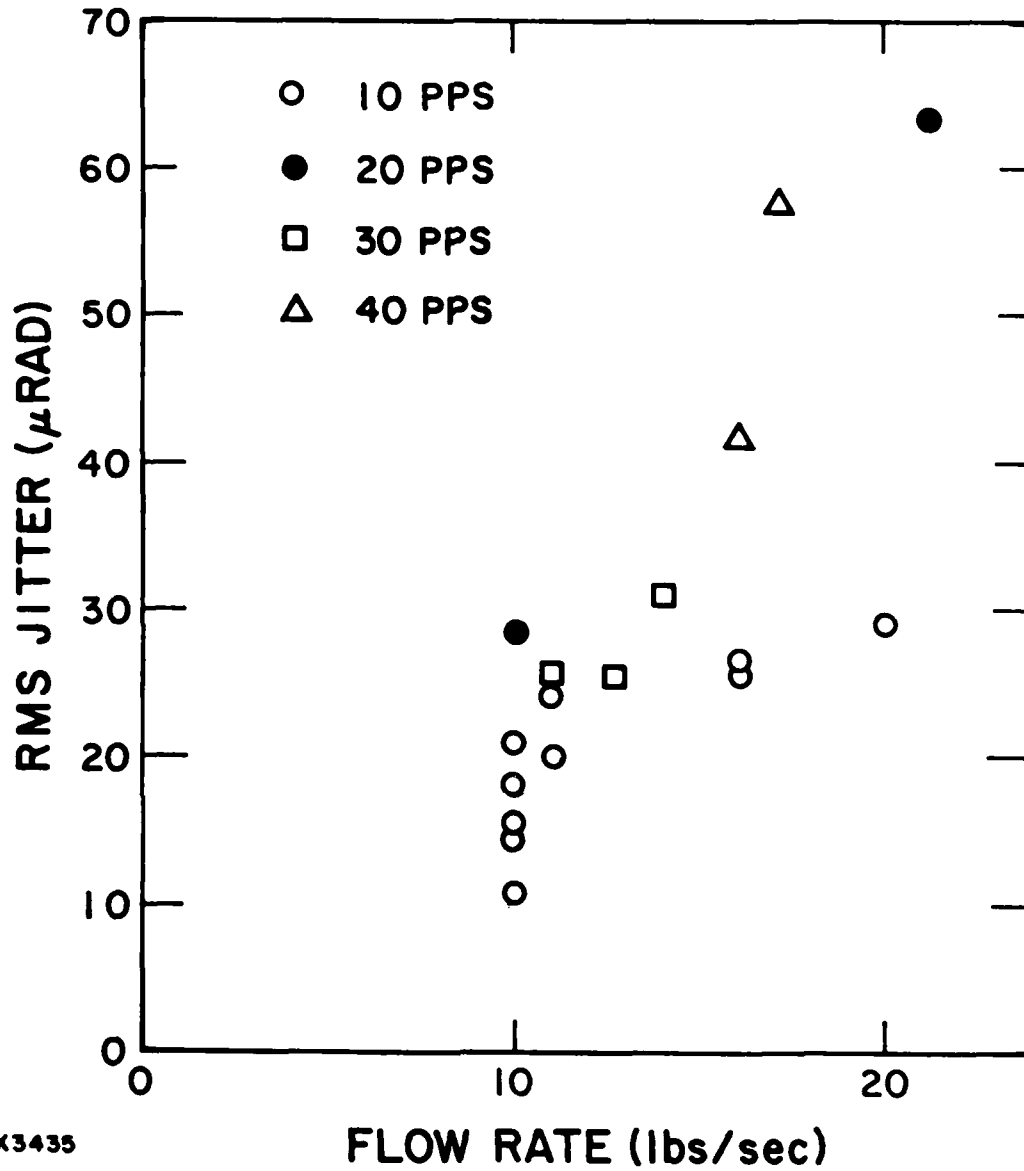
N ₂ :	CO ₂ :	H ₂ :	He
3	1	0.08	0.55

This gas has the property that its index of refraction matches the index of nitrogen which was the only gas available for aerowindow flow at the time of these tests. (This was because of the refurbishment of the ABEL-Humdinger gas facility.) The tests, therefore, test all beam steering contributions except the potential index change from aerowindow to room air when a non-index matched gas such as 3He: 2 N₂: 1 CO₂ are used.

In the core cavity configuration (with two salt windows), the IR jitter was measured for several flow rates and rep-rates. Figure 9 shows the measured flow rate dependence of the IR jitter. Data with rep-rates from 10 to 40 pps is shown. The trend of increasing rms jitter with increasing flow rate is evident.

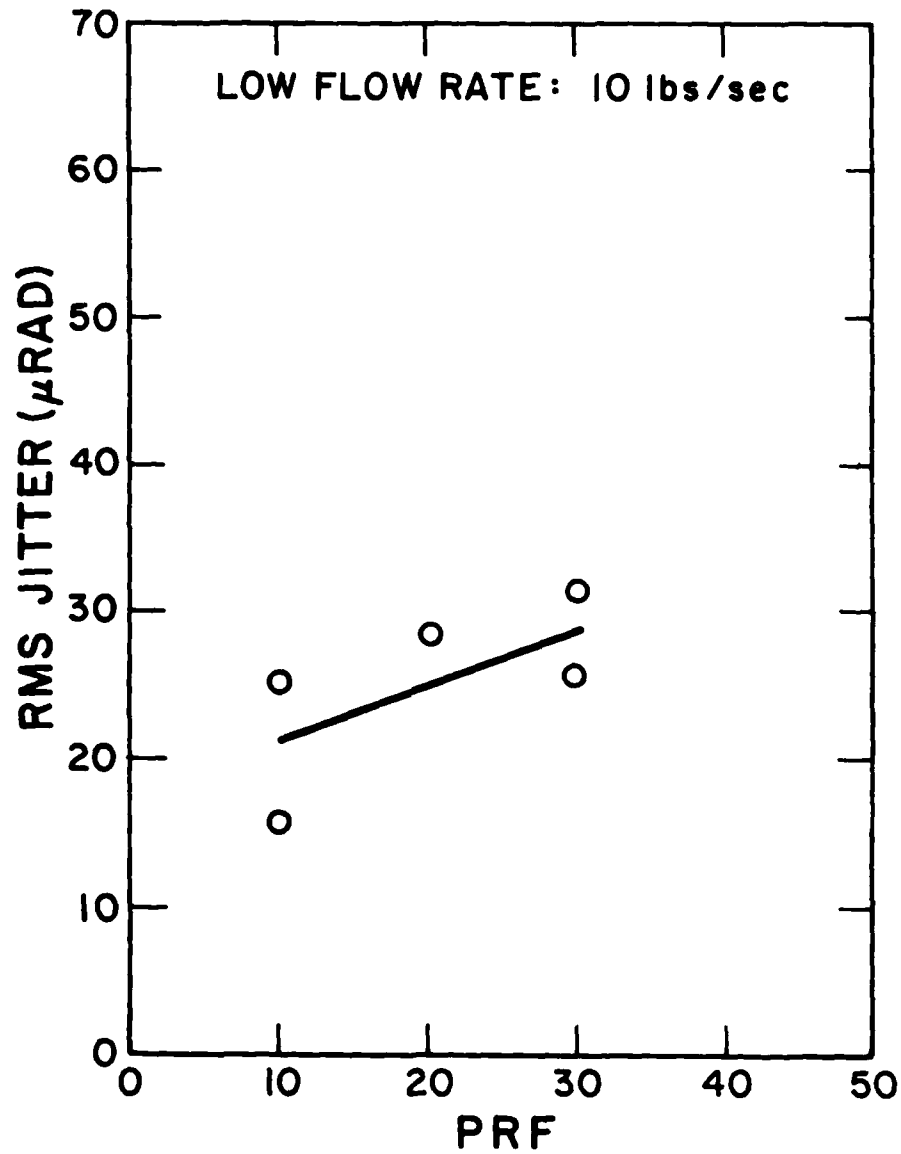
Figure 10 shows the rep-rate dependence of the IR jitter at low flow rates. Figure 11 shows the dependence at high flow. In both figures an increase of jitter with increasing rep-rate is apparent. Clearly both flow and rep-rate play a role.

Figure 12 shows the jitter dependence on the discharge energy loading. The effect is not large, the variation being not much larger than the scatter in the measurements. This weak loading dependence is evidence that the jitter is not caused by air breakdown effects of the high intensity IR laser beam. Some sparkling in the air along the beam path is visible at high power, but not at low power. The sparkling is apparently luminescence of dust particles in the beam path which doesn't affect the jitter significantly. This interpretation is also supported by the visible beam data in Section 5.0.



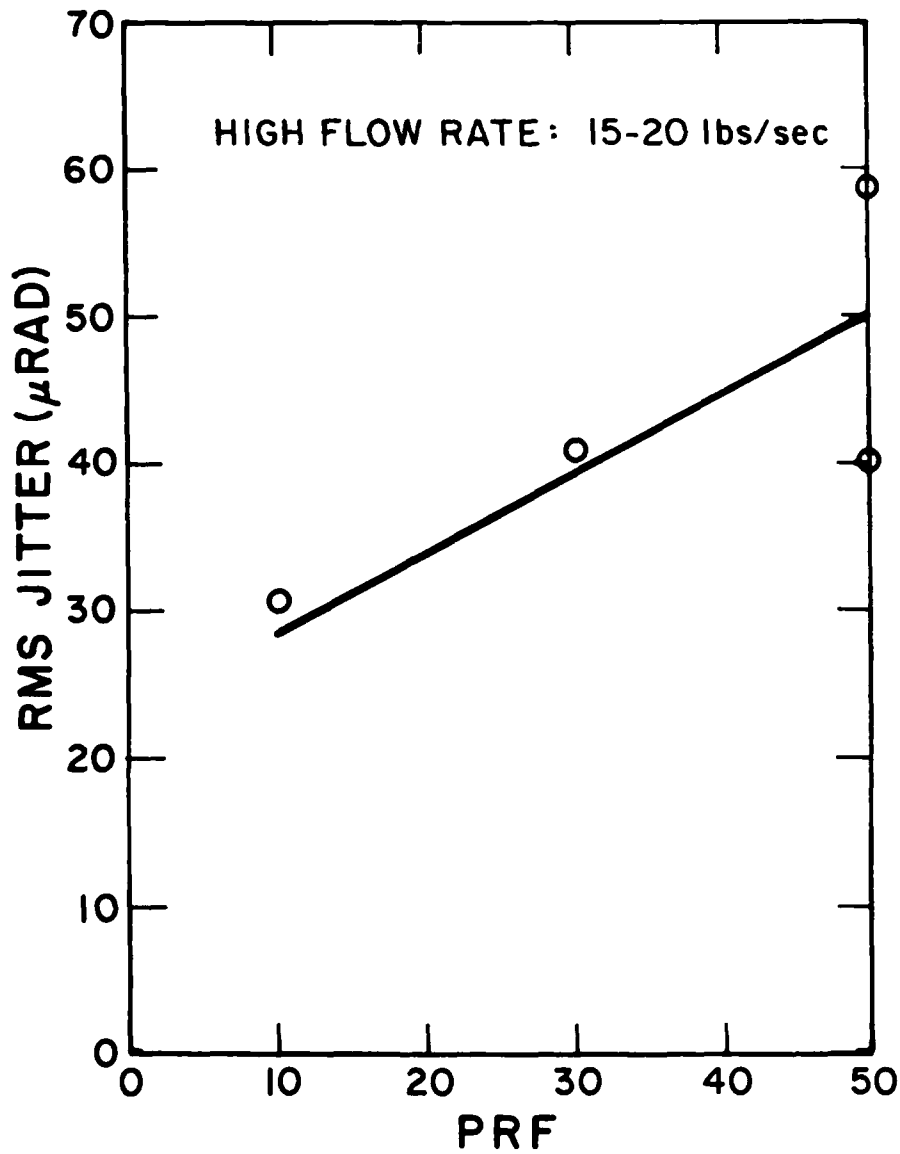
K3435

Figure 9. IR Jitter Dependence on Cavity Flow Rate; Cavity Core Flow with Salt Windows. Each point represents one 10-20 pulse laser burst at rep-rates between 10 and 40 pps.



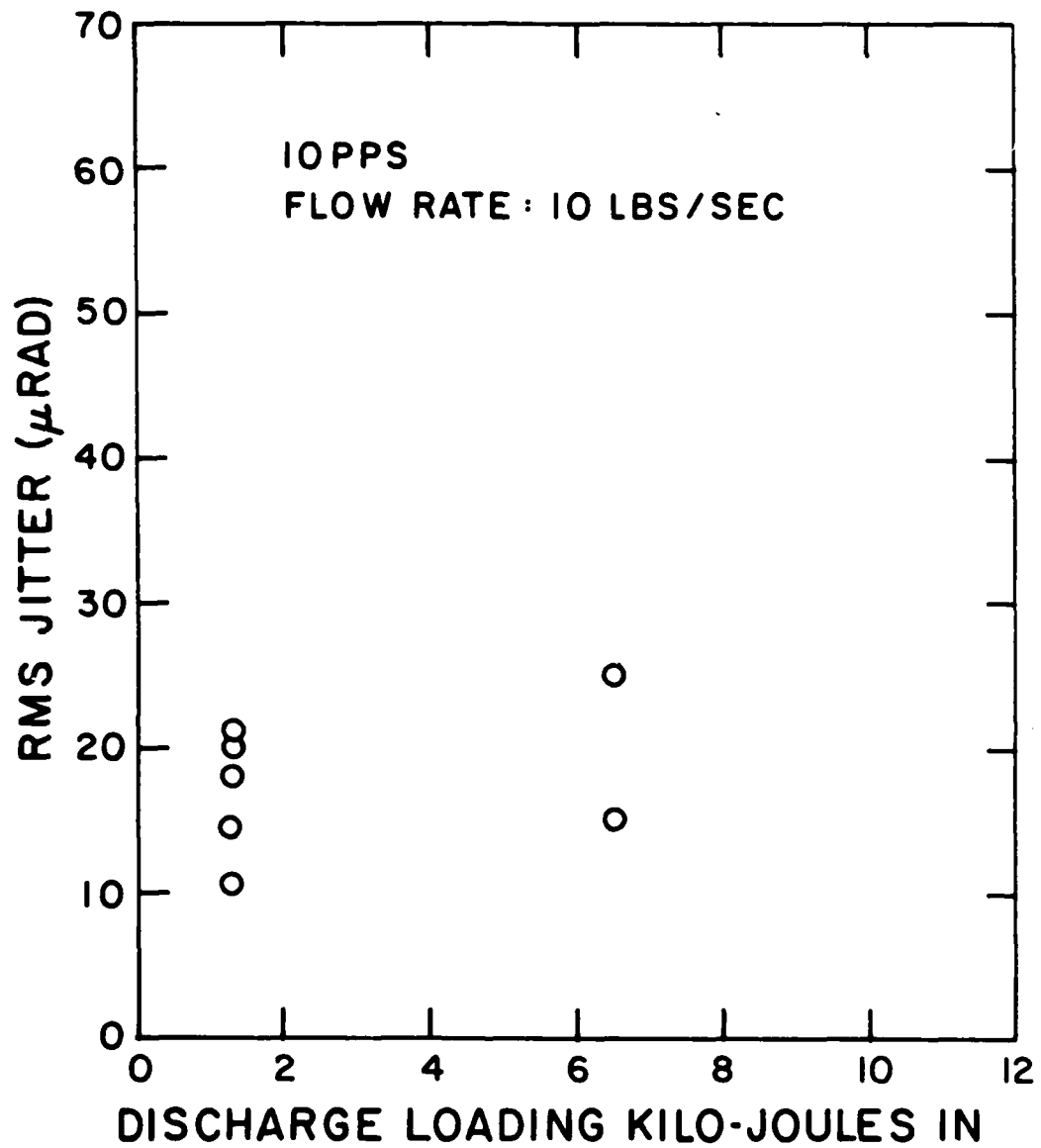
K3434

Figure 10. IR Jitter Dependence on Rep-Rate at Low Flow Rate; Cavity Core Flow with Salt Windows. Each point represents one 10-20 pulse laser burst.



K3434

Figure 11. IR Jitter Dependence on Rep-Rate at High Flow Rates (15-20 lbs/sec). Each point represents the rms jitter of one 10-20 pulse laser burst.



K3437

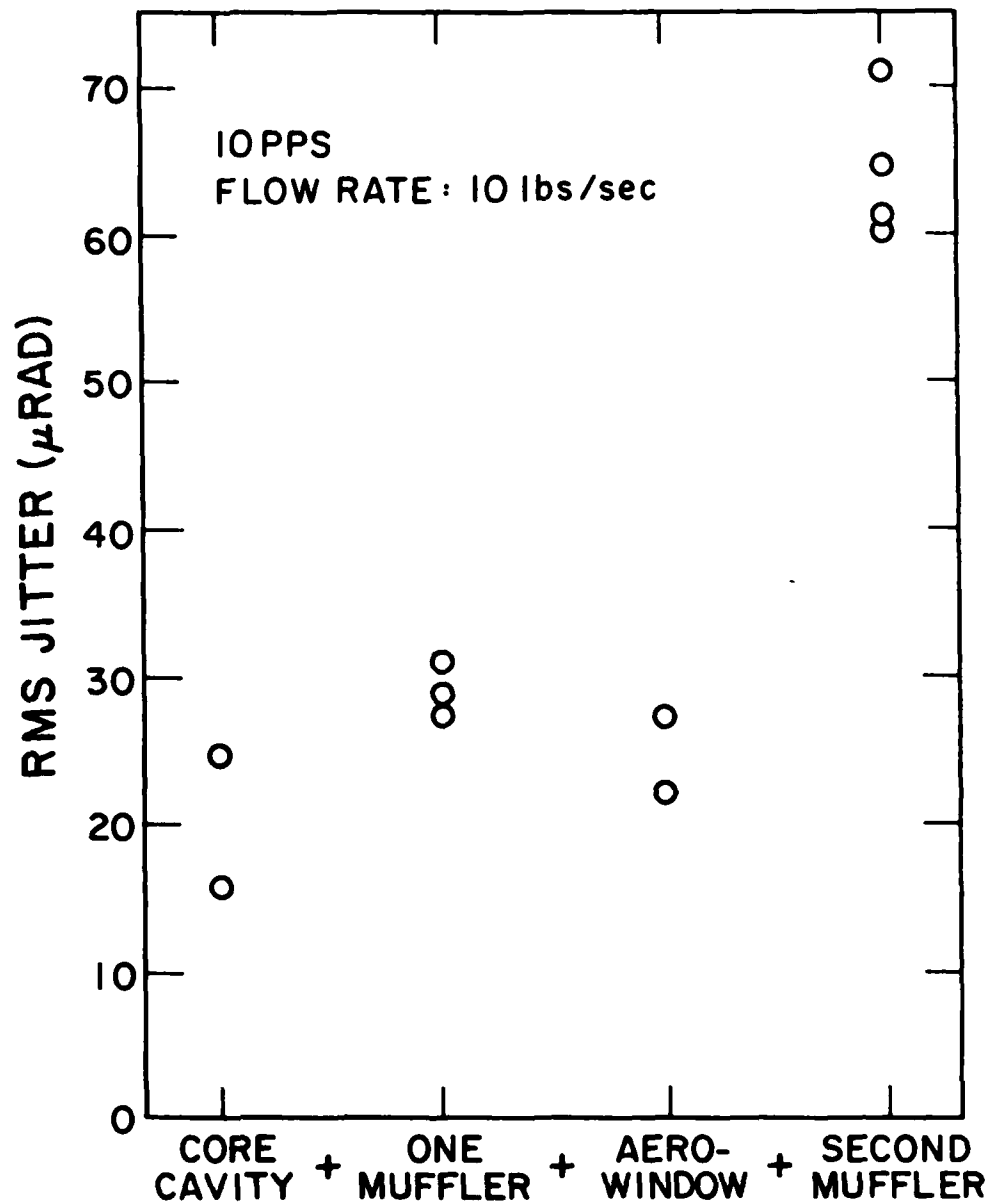
Figure 12. IR Jitter vs. Discharge Loading; Cavity Core Flow with Salt Windows. Each point represents one 10-20 pulse laser burst.

Figure 13 shows IR jitter data for four different laser component configurations. The first, configuration core cavity was with two salt windows on the laser cavity. Then one muffler was added (at the output or aerowindow end of the laser). Again two salt windows were used. Next the aerowindow replaced one of the salt windows. Finally, the other salt window was removed and the second muffler (at the primary mirror end of the cavity) was installed and tested.

Each component change affected the rms jitter. One muffler plus aerowindow produced much more jitter than the core cavity. Clearly there is a problem with the second muffler which mates the cavity with the primary mirror.

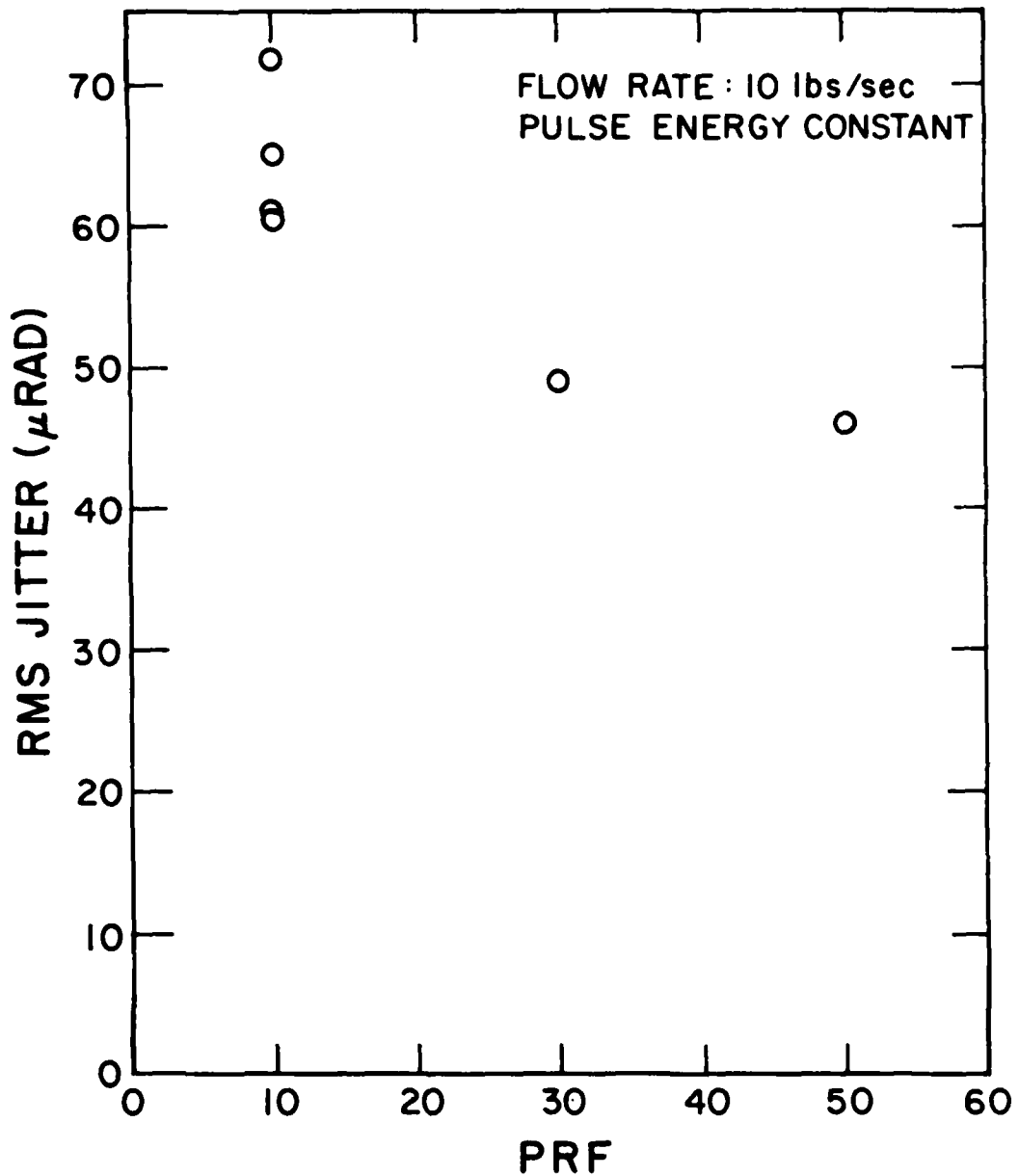
The effect of increasing the rep-rate in the second muffler plus aerowindow configuration was studied and the effect contrasts with that observed earlier for the core cavity. Figure 14 shows that increasing rep-rate decreases the jitter.

This rep-rate effect is the opposite of that observed for the cavity core flow with salt windows (Figures 10 and 11). As we shall show in the visible beam characterization data later, this muffler jitter is a "flow only" effect. It is likely that it is caused by a thermal boundary layer over the primary mirror surface.



K3436

Figure 13. IR Jitter as Mufflers and Aerowindow are Added to Coreflow. Data is for 10 pps, 10 lbs/sec flow. Each point represents one burst of 10-20 pulses.



K3432

Figure 14. IR Jitter Dependence on Rep-Rate with Two Mufflers and Aerowindow. Each point represents one burst of 10-20 pulses.

5.0 VISIBLE CHARACTERIZATION DATA

The visible probe beam data and reference data presented here were obtained using the measurement techniques described in Section 2.2. These tests were performed with no CO₂ in the gas mix to suppress lasing. Most were run with N₂ only, some were run with a He mix (1He:1N₂) to simulate the 3He:2N₂:1CO₂ mix (with the CO₂ replaced with N₂).

In Figures 15 - 18 the measured beam coordinates are plotted for some of the tests. These time histories of the beam coordinates are plotted for both short (~ 10 msec) and long (~ 1 sec) time periods for beam motion between pulses and pulse-to-pulse beam motion. The latter simulates the IR pulse-to-pulse beam jitter.

Looking first at a sample of the cavity beam during flow before the pulsing starts (Figure 15) we see that the flow only jitter is dominated by the Y, or vertical, component. The Y-axis is along the flow direction. Note that for comparison with the IR confocal resonator jitter the total jitter σ_t of 7.77 should be multiplied by 1.75 as discussed in Section 2.2. The equivalent resonator jitter would thus be 13.6 μ rad (assuming the beam steering is dominated by the laser cavity).

A temporal plot of the reference beam over the same time frame as the above is shown in Figure 16. The total reference beam jitter is 3.15 μ rad. If the cavity beam motion is the result of two independent random sources, i.e., (1) the laser cavity and (2) thermal gradients in the room, the rms jitter of the two effects is combined as the square root of the sum of the squares of the individual components:

$$\sigma_{\text{tot}} = \sqrt{\sigma_{\text{laser}}^2 + \sigma_{\text{thermal grad}}^2}$$

The magnitude of correction based on the reference measurement in this case would be:

$$\sigma_{\text{laser}} = \sqrt{\sigma_{\text{tot}}^2 - \sigma_{\text{ref}}^2}$$

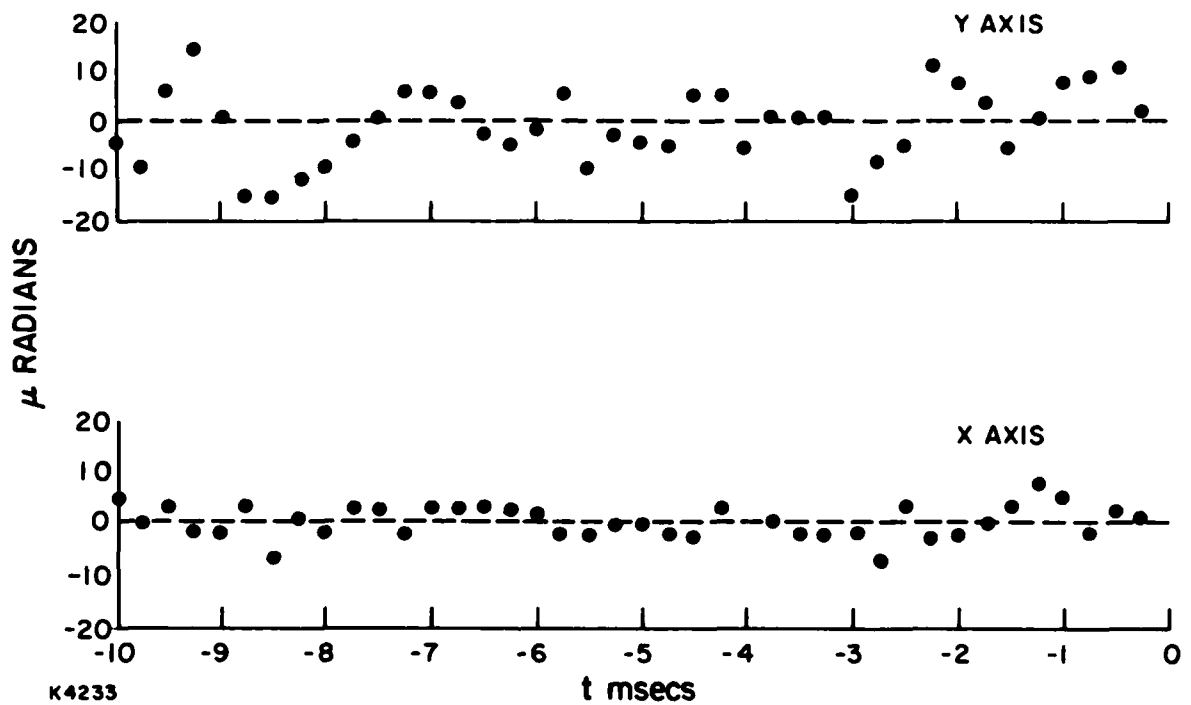


Figure 15. Cavity Beam During Flow Before First Pulse $\sigma_x = 3.09 \mu\text{rad}$, $\sigma_y = 7.13 \mu\text{rad}$, $\sigma_{\text{tot}} = 7.77 \mu\text{rad}$. Flow rate 10 lbs/sec. Each point represents position of beam center in individual movie frames.

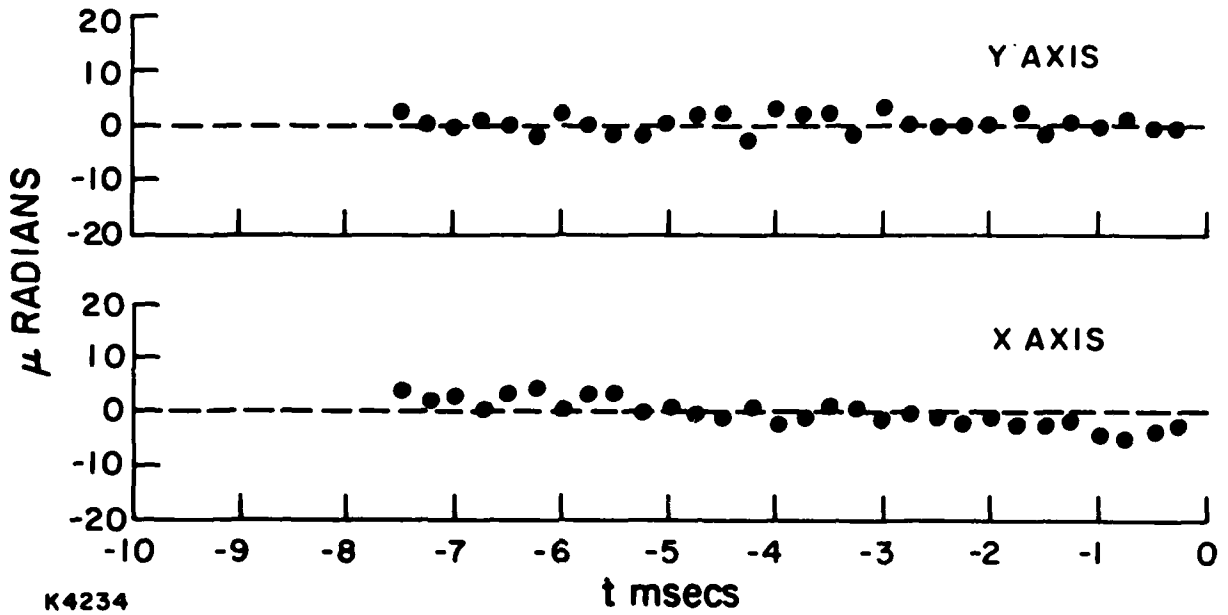


Figure 16. Reference Beam Before First Pulse $\sigma_x = 2.30 \mu\text{rad}$,
 $\sigma_y = 2.15 \mu\text{rad}$, $\sigma_{\text{tot}} = 3.15 \mu\text{rad}$.

$$\sigma_{\text{laser}} = \sqrt{7.77^2 - 3.15^2}$$

$$= 7.10$$

The jitter is clearly dominated by the laser cavity. This was true for all the tests examined for both the short and long time scales. In the data that follows, no numerical correction for the external contribution to the beam jitter is made. Since a good portion of the reference beam path is through additional room air beyond what the cavity beam sees, the actual correction should be substantially smaller than the measured reference beam jitter. Subtracting the reference beam coordinates from the cavity beam coordinates at each point in time is not done for this reason. The contribution from the co-incident beam paths would be removed by the subtraction, but the jitter from the extra beam path of the reference beam would also be subtracted. For our purposes however the cavity beam data without external path corrections is sufficient.

In Figure 17 a sample of pulse-to-pulse cavity beam jitter as measured with the visible probe beam is shown over a period of 20 pulses. At each pulse the beam coordinates are taken from the last movie frame before the pulse. This presumably would be the location of an actual laser pulse. The total measured rms jitter of 12.9 μrad corresponds to a confocal resonator jitter of 22.6 μrad .

Reference beam measurements for the same 20-pulse time period indicate a reference beam rms motion of 5.96 μrad . This implies that the actual laser cavity jitter is between 11.4 and 12.9 μrad . A reference beam measurement on a similar time scale during the flow before the first discharge pulse indicated a motion of 4.50 μrad . The reference beam is, therefore, only slightly affected by the discharges. In both the flow only and flow plus discharge cases, the mirrors and room air are stable enough for us to measure directly the dominant laser cavity jitter.

The pulse-to-pulse cavity beam measurements discussed above utilized at the last movie frame before each pulse. Immediately after each discharge pulse the focal image on the film disappeared out of the field of view and recovered as plotted in Figure 18. The deflection of the beam was predominantly in the horizontal plane representing a beam deflection toward the cathode of 200 μrad . This is attributed to the asymmetry in the Humdinger cavity with a solid anode on one side and an open cathode consisting of an array of tubes on the other. This can result in both acoustic and thermal asymmetries after the discharge. The acoustic effect results from the unequal attenuation of the shock waves on the two sides. The thermal gradient results from the mixing of the volume of cold gas behind the cathode rods with the hot gas across the cavity. The cooler (denser) gas toward the cathode would shift the beam in the direction observed. This systematic beam motion is not jitter and should pose no problem for beam pointing precision.

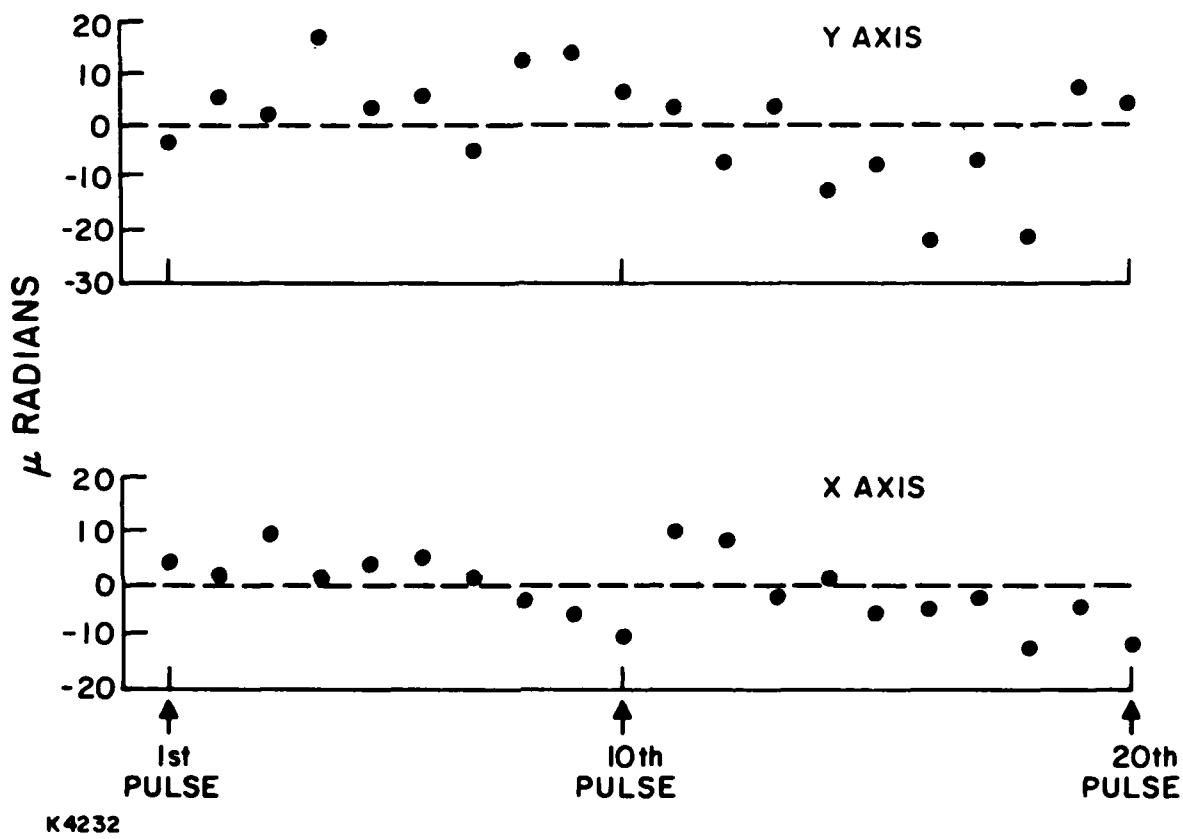


Figure 17. Pulse-to-Pulse Cavity Beam Jitter. $\sigma_x = 6.89 \mu\text{rad}$,
 $\sigma_y = 10.90 \mu\text{rad}$, $\sigma_{\text{tot}} = 12.9 \mu\text{rad}$. Flow rate 10 lbs/sec,
 10 pps.

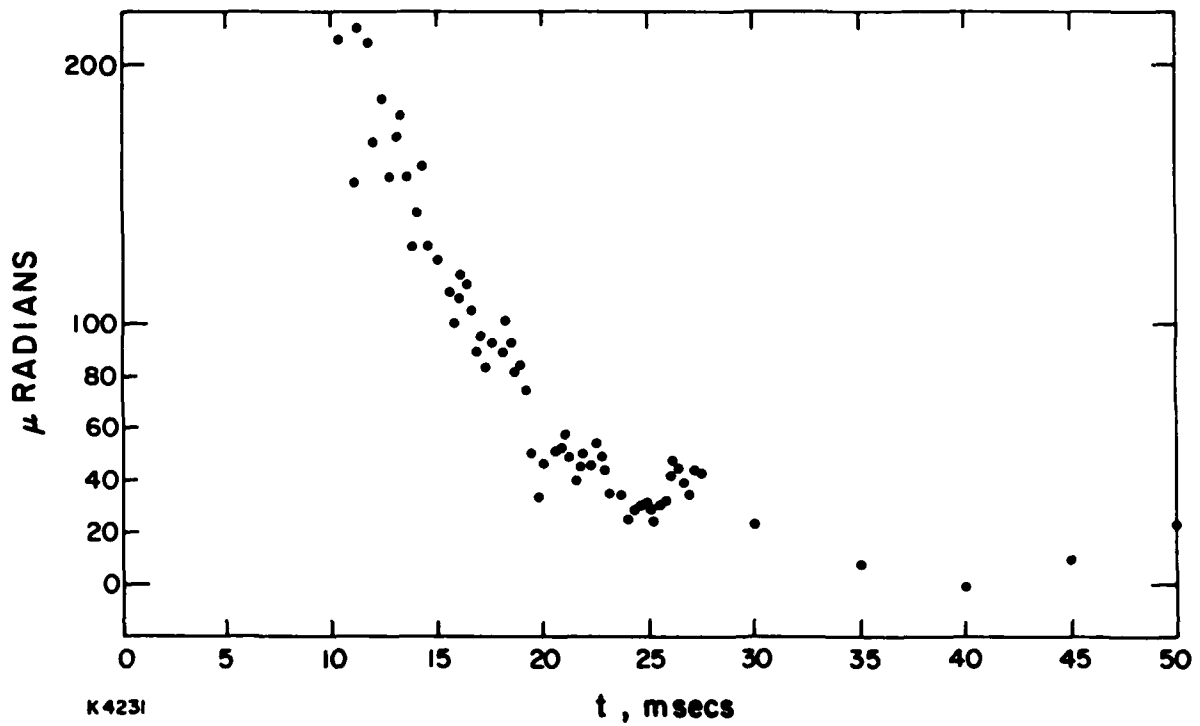


Figure 18. Recovery of Cavity Beam After First Pulse. Each point represents x coordinate of focal spot in one movie frame. Framing rate 4000 fps. After 27 msec each 20th frame was measured. Flow rate 10 lbs/sec.

Next, we measured the pulse-to-pulse visible beam jitter for various conditions for comparison with the IR data. Figure 19 shows the pulse-to-pulse visible probe beam jitter as a function of flow rate. The configurations were flow only, and pulse repetition rates of 10 to 30 pps. The data was obtained by measuring the beam position on the movie frame just before each pulse. For the flow only data a time interval of 1/10 of a second between frames measured was used. For comparison with the IR (confocal resonator) results this data is multiplied by 1.75 and replotted in Figure 20. This plot is similar to the IR plot in Figure 9. In both the jitter is about 20 μ rad at low flow rates increasing by a factor of two to three at the higher flow rates.

Figure 21 compares the measured IR jitter with the corrected visible beam jitter. All the runs at 10 pps with 10 lb/sec flow rate were averaged for the IR and then plotted against the average for all the visible runs under similar conditions. Thus, one point is plotted. The brackets represent the spread in measurements between the individual runs. The two measurement methods yield jitter magnitudes nearly equal, the visible jitter being slightly higher. This is attributed to the difference in the aperture diameters, 4.5 cm for the IR, 1.3 cm for the visible.

One would expect in general that smaller samples of the same beam would tend to exhibit greater angular jitter than for the full beam. This is because, when the individual portions are combined to form the far field pattern of the full beam, some of the jitter of the individual pieces will tend to average out. In effect, uncorrelated motion of different parts of the beam will be converted to fluctuations in beam quality and focal point shape. The exact scaling would depend on the scale size and form of the particular mechanisms involved in refracting the beam. Our experience on this device indicates that the angular jitter is a very weak function of aperture size over the diameter range 1-9 cm.

The correlation of the visible jitter with the IR jitter is important as it establishes that the beam motion is not caused by beam breakdown in the air, thermal blooming, or other nonlinear effects related to the high-power beam propagation or beam extraction process. It is a medium effect in the laser gas.

In order to help sort out the effects of the flow and the repped discharge on the beam motion, the data in Figure 22 was plotted. Plotted at 0 pps is the data taken during the flow before pulsing started. The flow data for each run is connected with a straight line to the data obtained after the pulsing started. In each case the repped discharge increased the beam jitter over the core flow jitter substantially. The variations of flow-only jitter from run-to-run are due in part to the fact that different flow rates were used for the various runs. Even among runs at the same flow rate there are substantial run-to-run variations however.

Next we look at the visible beam jitter as the mufflers and aerowindow are added to the core cavity in Figure 23. No difference in the jitter magnitude was apparent as one muffler and then the aerowindow were added. The one

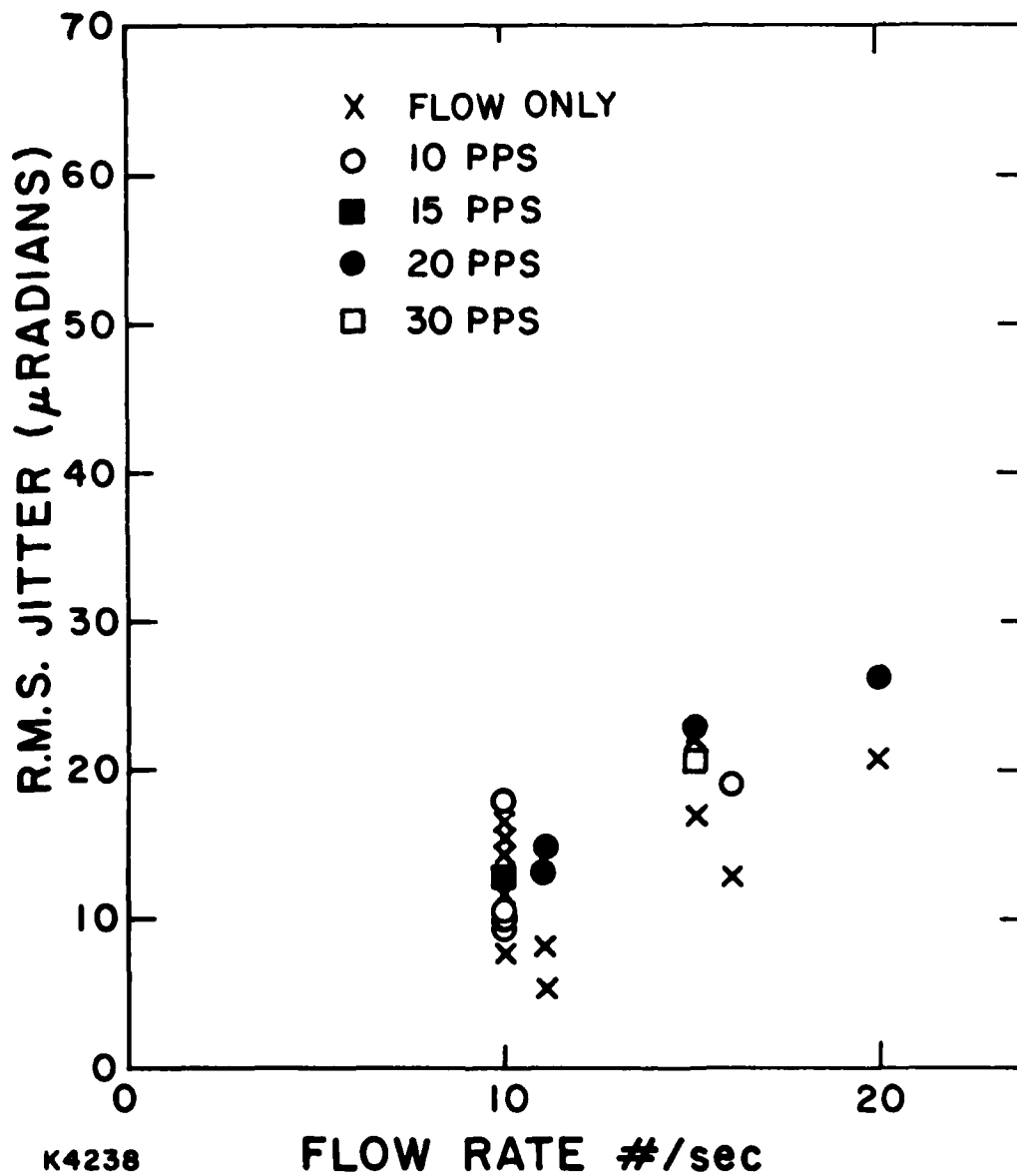


Figure 19. Pulse-to-Pulse rms Jitter of Visible Probe Beam vs. Flow Rate.

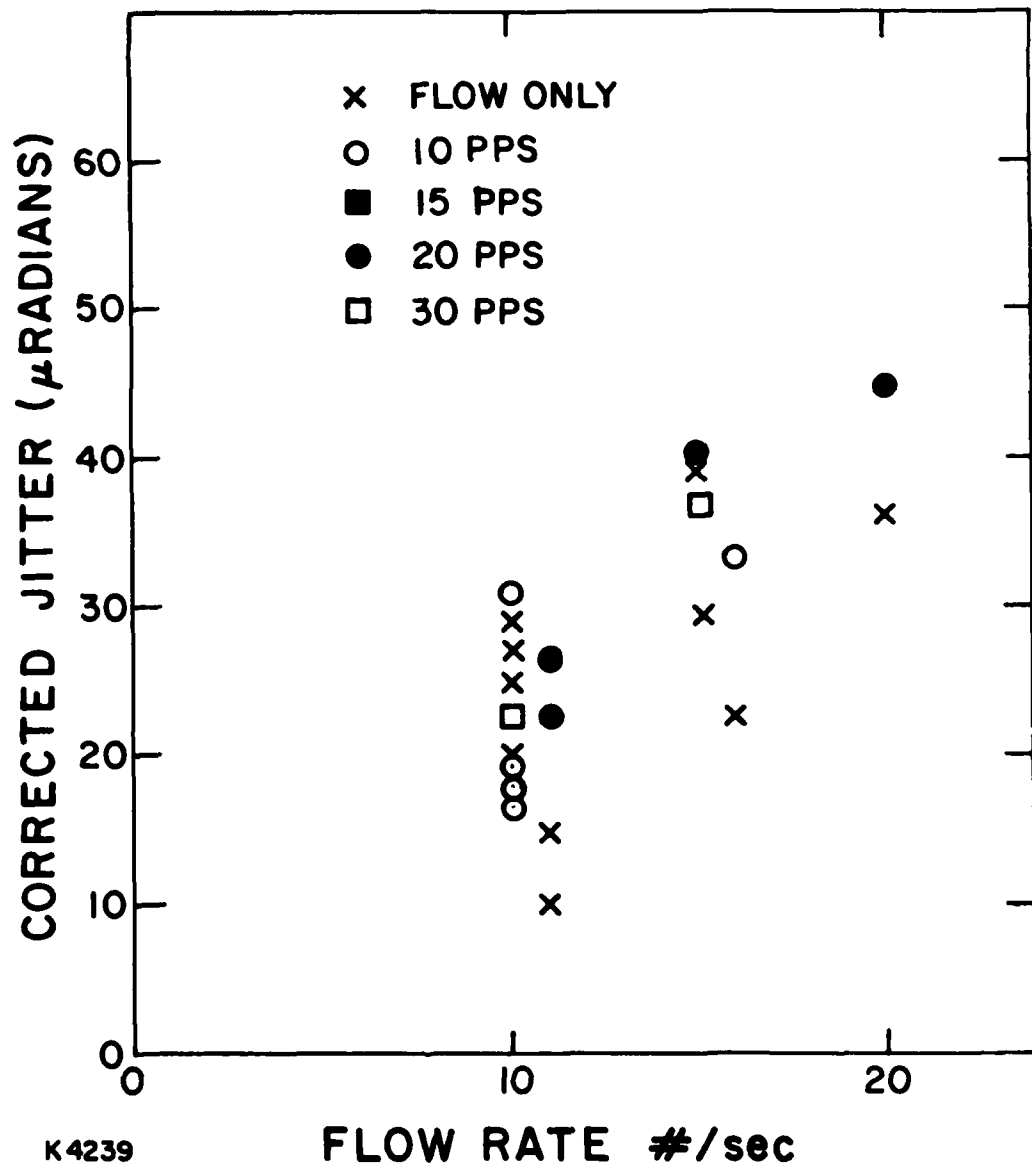


Figure 20. Visible Probe Beam Jitter Corrected by Confocal Resonator Factor of 1.75.

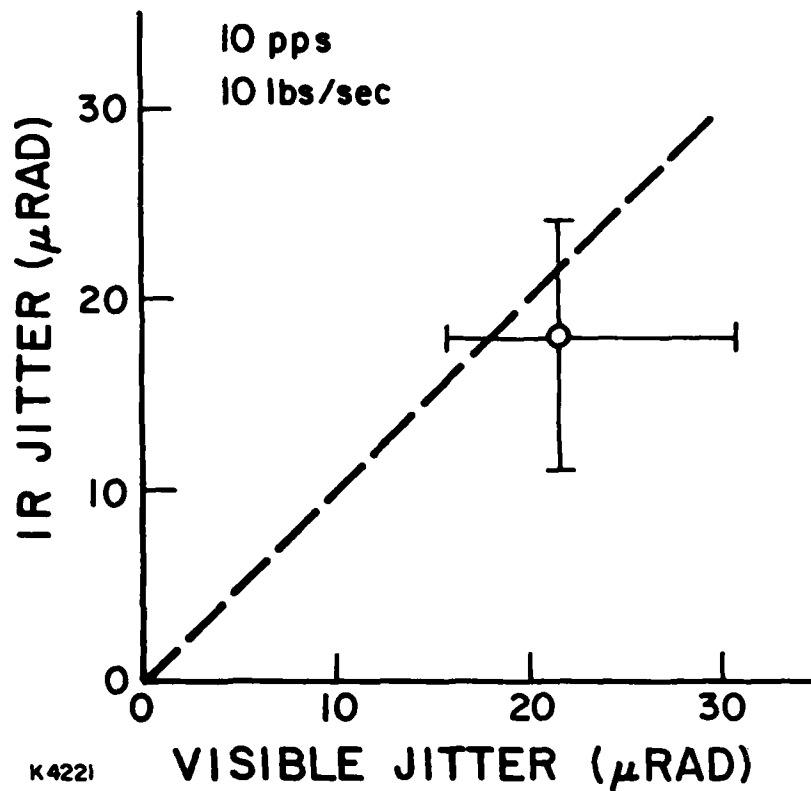
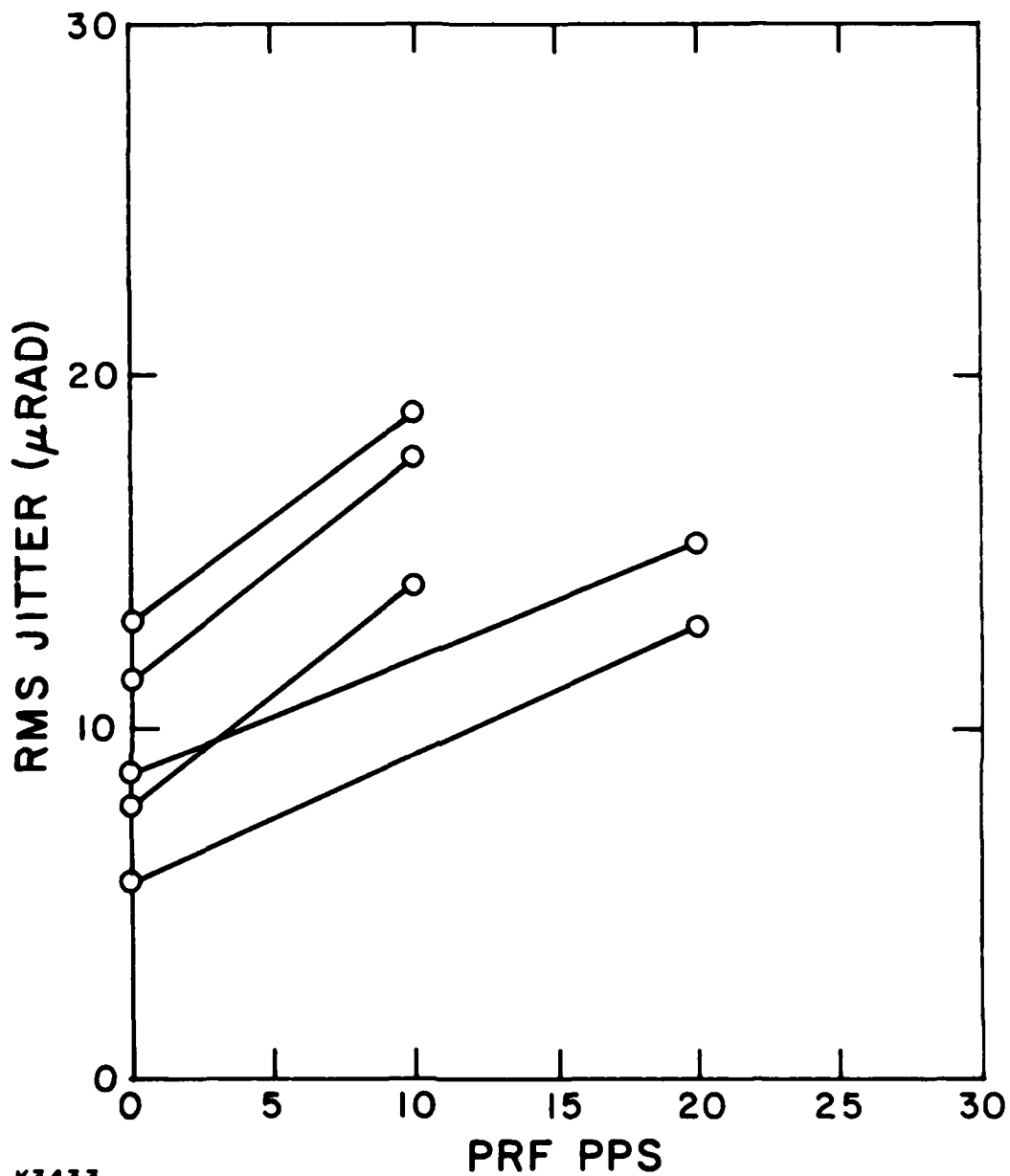
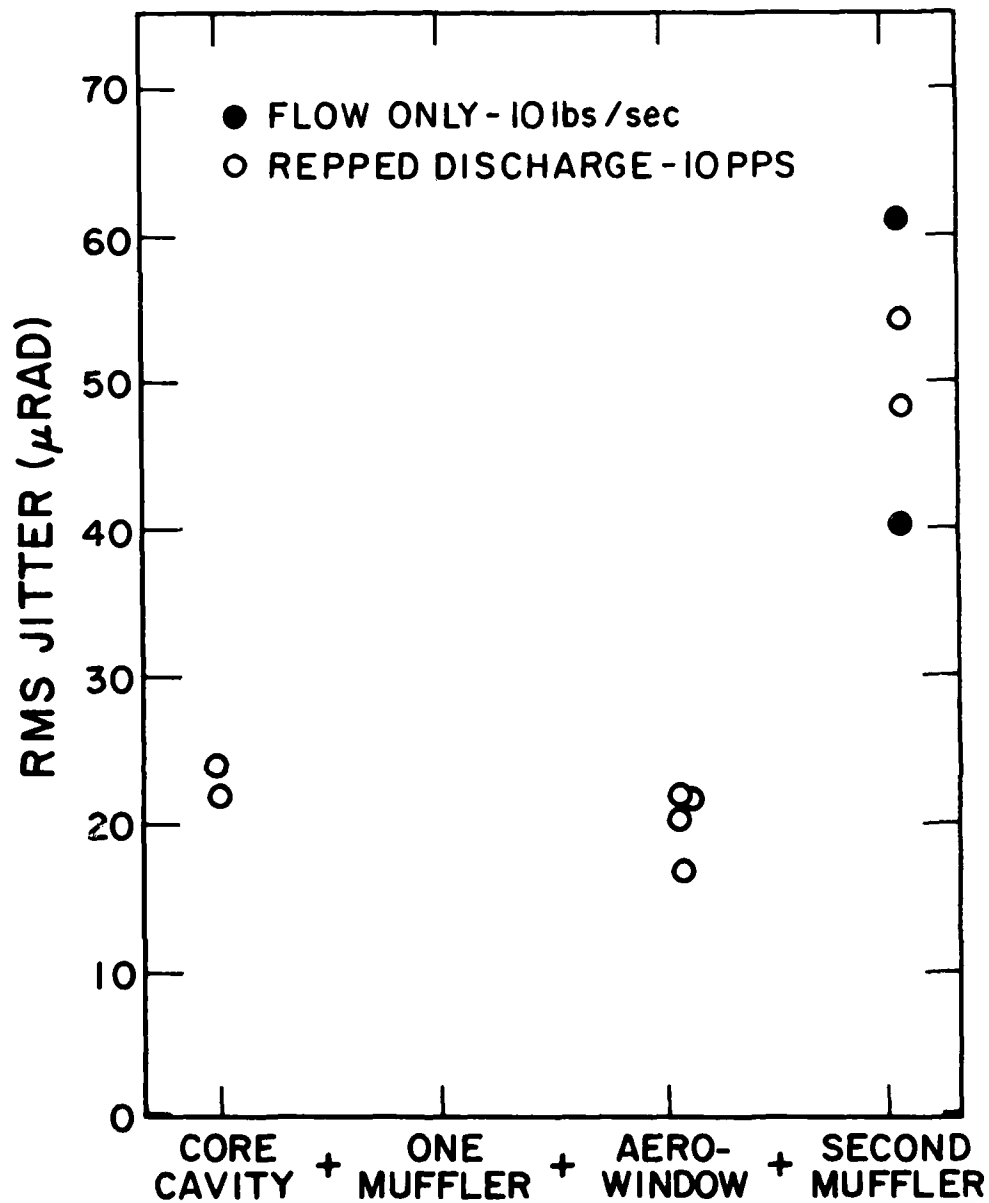


Figure 21. Comparison of IR Jitter With Visible Jitter. Average of rms jitter for a number of runs is plotted. Brackets represent spread in data.



K3433

Figure 22. Effect of Repped Discharge on Visible Beam Jitter. Each line represents one run. The point on the left end of the line is the jitter before the repping began. The point on the right end of the line shows the level of jitter with repping in progress.



K3436-1

Figure 23. Visible Probe Beam Jitter as Mufflers and Aerowindow are Added. Data is corrected with confocal resonator factor of 1.75.

muffler (aerowindow end) data was recorded with the TV video recorder and is not plotted here with the movie data. This did show the same jitter magnitude as the core cavity data as measured with the TV camera. As with the Ik measurements (Figure 13) the second muffler (at the primary mirror end) increases the beam motion substantially. The flow only measurements with the second muffler are as high as the measurements with the repped discharge. This muffler effect is thus a flow effect, probably a thermal boundary layer over the primary mirror. This is likely because there is a transition section with flow connecting the primary mirror with the muffler section in Humdinger. This dead gas region in front of the mirror is about 10 cm long. The source of this thermal boundary layer may be the temperature difference between the flowing gas in the cavity and the mirror surface.

6.0 TEMPERATURE MEASUREMENTS

Thermal gradients in the gas across the beam path can cause beam deflection so some measurements of the gas temperature at several points in the flow system were performed. The gas system is shown in Figure 24.

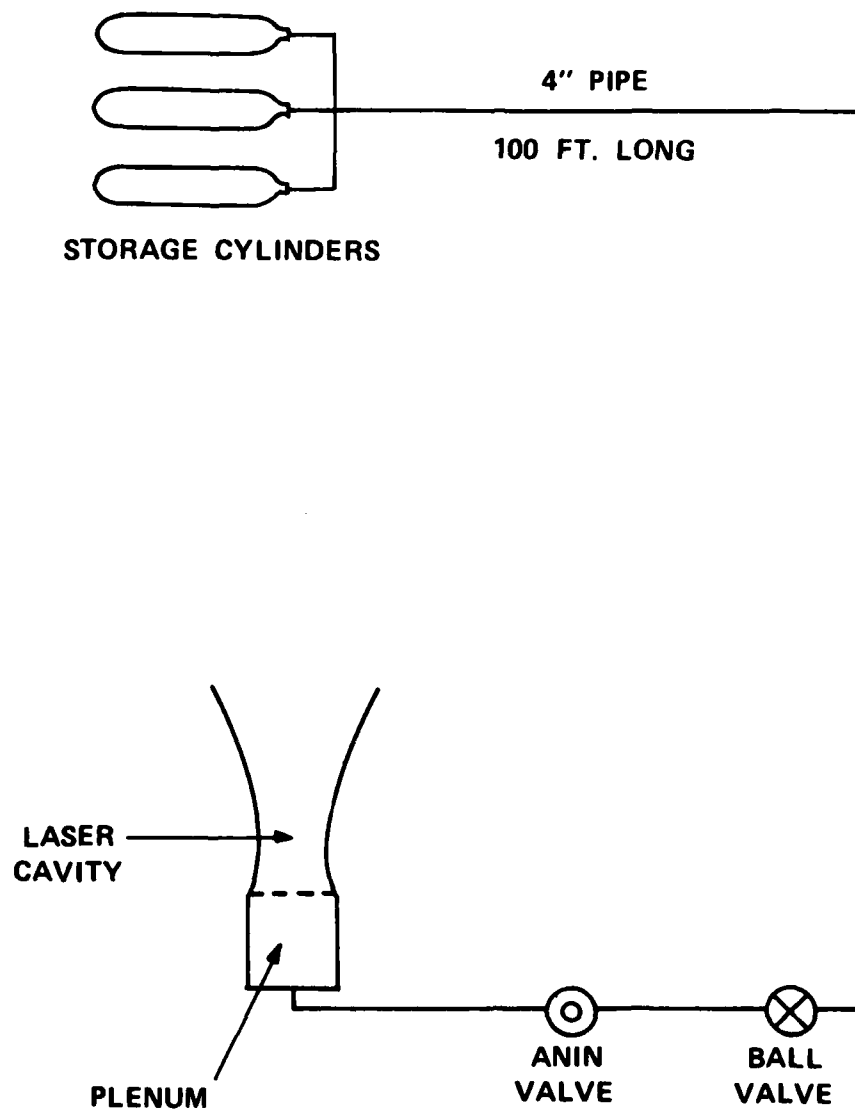
The mixed gas is in cylinders at ~ 2000 psi. The gas is fed via a 4 in. pipe (~ 100 ft long) to a ball valve and control orifice (Anin valve) where the flow rate is regulated and the pressure drops to slightly above atmospheric pressure. An 8 in. pipe carries the gas to the laser plenum entrance where a set of orifices distribute the gas along the plenum and introduce another pressure drop (50-100 psi). The adiabatic expansion of the gas at each pressure drop results in a reduction in the gas temperature below the temperature of the pipe, plenum and cavity. The difference in temperature between the walls and gas can result in fluctuating thermal gradients in the delivered gas flow.

For a flow rate of 10 lbs/sec the gas temperature dropped from 57°F (upstream of the regulating valve) to 41°F in the cavity. At 20 lbs/sec the gas temperature dropped to 32°F in the cavity.

Some differential thermocouple measurements were also made to get an idea of the magnitude of the thermal gradients in the laser cavity. Two thermocouples were placed in the cavity 7 cm apart first with a horizontal displacement (transverse to the flow) and then with a vertical displacement (along the flow). The thermocouples were 0.001 inches in diameter with a time response in a 10 m/sec gas flow of better than 1 msec. The thermocouple junctions were wired to measure the difference in temperature between the two points. Figures 25 and 26 show recordings of the differential thermocouple measurements with horizontal and vertical displacement. Fluctuations of the order of 1-2°F are evident with a frequency of the order of 25-50 Hz.

A $\Delta\rho/\rho$ or $\Delta T/T$ averaged over the beam path through the laser cavity with the $3N_2:1CO_2:0.08H_2$ gas mixture will cause a deflection of the IR beam through an angle

$$\sigma = \frac{(n - 1) L}{w} \left(\frac{\Delta\rho}{\rho} \right) \times \frac{R_1}{R_1 - R_2}$$



K 6578

Figure 24. Humdinger Gas System

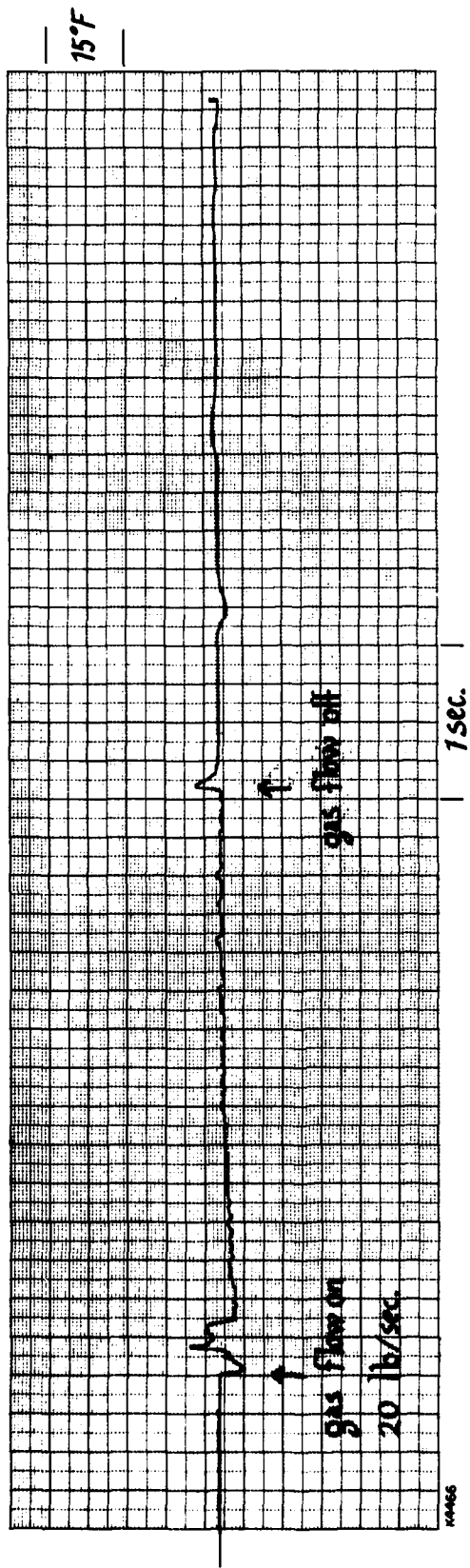


Figure 25. Differential Thermocouple Recording, Horizontal Displacement

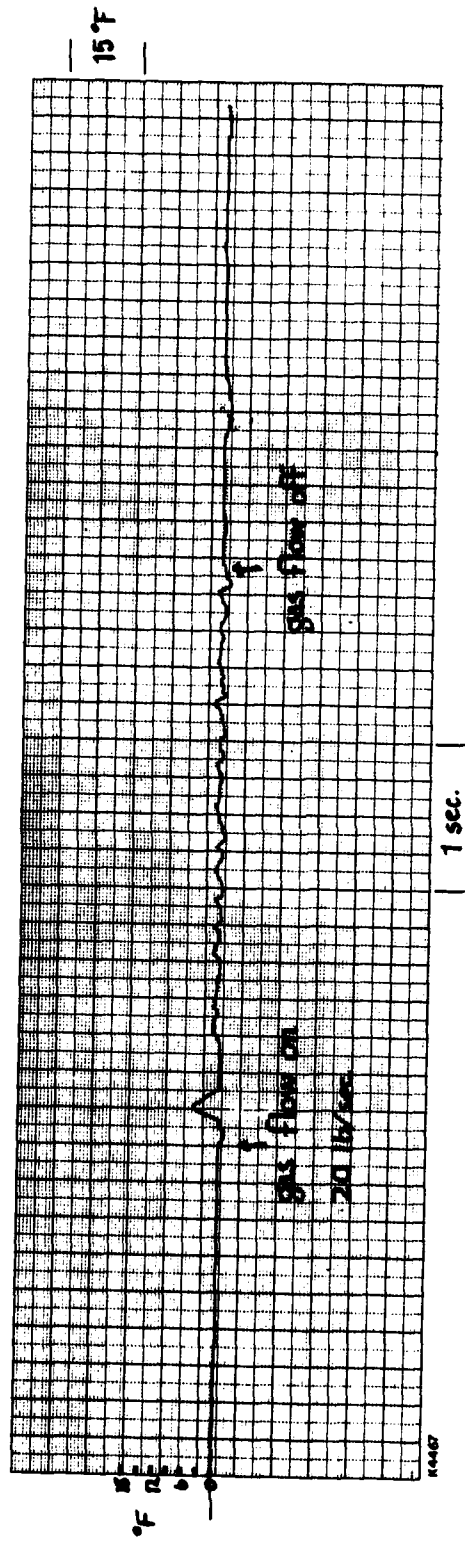


Figure 26. Differential Thermocouple Recording, Vertical Displacement

where

W is the cavity width (10 cm)

R_1 and R_2 are the radii of curvature of the resonator mirrors (28 m, 12 m)

L is the round trip beam pathlength (6 m)

n is the index of refraction (1.0003)

$R_1/(R_1 - R_2)$ is the magnification factor calculated earlier for the confocal resonator. This factor is multiplied times the difference in effective path length for rays at the two sides of the cavity $(n-1)L \Delta\rho/\rho$ and divided by the width of the cavity W to obtain a deflection angle.

For the 3 meter cavity length, an average ΔT of 1°F between anode and cathode results in

$$\sigma = 58 \mu\text{rad}$$

The thermal gradients in the gas must therefore be controlled to a small fraction of a degree.

One approach to reducing the potential for thermal gradients is to adjust the gas temperature in the plenum and pipe to match the wall temperature. This can be accomplished by heating the gas to compensate for the adiabatic cooling. For Humdinger the storage cylinders are housed in a separate shed so the temperature of the stored gas can be varied independently. It was discovered however that the gas temperature at the regulating valve was independent of storage temperature over a wide range (30°F to 100°F). The temperature of the 100-foot length of 4 in. pipe effectively regulates the gas temperature. The gas temperature can therefore be controlled by controlling the temperature of this pipe to compensate for the downstream adiabatic cooling. This method was evaluated by wrapping the 4 in. pipe with heating tape and insulation. The cavity gas can now be delivered at room temperature (or higher) by setting the upstream pipe temperature to 90°F.

Measurements of beam jitter were not performed with temperature control. Visible beam tests with flow only as a function of gas temperature should be enlightening however.

7.0 CONCLUSION

Diagnostic techniques for measuring pulsed IR beam jitter and for doing probe beam medium characterization and mirror monitoring were tested. The technique of recording the central peak of the beam with the shadow of a cross hair on a thermal image is straightforward. Displacements of the peak of the focal spots down to 3 μ rad were measured.

This technique of measuring the jitter using the fluence profile near the peak is more appropriate than measuring the centroid of the whole pattern, if one is interested in the question of damage to targets at long range with the peak portion of the distribution.

The visible probe beam tests showed that the visible jitter was approximately equal to the IR jitter. It will be a valuable technique therefore for diagnostic purposes in determining sources of jitter in a laser system.

In addition to establishing these techniques the data taken on the Humdinger laser was analyzed to identify and discriminated between sources of jitter in a representative pulsed flowing system. The conclusions for this particular system were the following:

1. The mirrors were adequately stable and did not move significantly during repped discharges.
2. The beam jitter ranged between about 15 μ rad and 70 μ rad under various conditions.
3. The visible beam tests established that the beam motion is not caused by air breakdown or thermal blooming in the beam path.
4. The base jitter of about 15 μ rad was associated with the core cavity flow.
5. Higher flow rates increased the jitter by about a factor of 2.
6. A component of the jitter is associated with disturbances from the pulsed repping as evidenced by the rep-rate dependence. At higher rep-rates (50 Hz) jitter increased to about 50 μ rad.
7. A major contribution to jitter was traced to the primary mirror muffler.

8. The source of the base core cavity jitter is probably cavity thermals in the gas. This source can be eliminated by stabilizing temperatures in the flow system.
9. The above jitter magnitudes are representative only in that the system was not optimized for these tests and only an apertured portion of the beam was studied. A full aperture beam would be expected to be better to some extent.

DISTRIBUTION LIST

Commander US Army Missile Command Redstone Arsenal, AL 35898 Attn: DRSMI-RHB, Dr. T.A. Roberts RHE, Mr. J.C. Walters RHC, Mr. K. Smith RHC, Mr. Myron Cole RHS, Dr. George Dezenberg	10 copies
Commander US Army Mobility Equipment R&D Command Ft. Belvoir, VA 22060 Attn: DRDME-R, Mr. Cooper EA, Dr. Larry Amsutz	2 copies
Defense Advanced Research Projects Agency 1400 Wilson Boulevard Arlington, VA 22209 Attn: Director, Laser Division	1 copy
Air Force Weapons Lab Kirtland AFB, NM 87117 Attn: AFWL/ARAY, LTC T. Meyer	6 copies
Defense Documentation Center Cameron Station Alexandria, VA 22314	12 copies
RSIC Redstone Arsenal, AL 35898	3 copies

END

FILMED

6-83

DTIC